博士論文

Fabrication of self-oscillating hydrogel containing magnetic nanoparticles and the regulation of dynamic behaviors

(磁性ナノ粒子を内包する自励振動ハイドロゲルの作製と
動的挙動の制御)

李　殷　種

Referee in chief:	Professor	Dr. Ryo Yoshida
Referee:	Professor	Dr. Kazuhiko Ishihara
	Associate Professor	Dr. Yuichi Yamasaki
	Associate Professor	Dr. Takamasa Sakai
	Lecturer	Dr. Aya Mizutani Akimoto

Acknowledgement

The present doctoral dissertation is the completion of works carried out at The University of Tokyo from October 2015 through September 2018 supervised by Professor Dr. Ryo Yoshida and Lecturer Dr. Aya Mizutani Akimoto at Department of Materials Engineering, School of Engineering, The University of Tokyo.

First of all, the author would like to express the deepest appreciation to Professor Dr. Ryo Yoshida for kindly welcoming the author as a member of his research group for 3.5 years including a research student, giving him persistent guidance and insightful suggestions, and giving him opportunities to attend domestic and international conferences and to collaborate with other institutes with financial support. Thanks to him, the author could acquire precious experiences, knowledge, and a philosophy. Therefore, the author was able to understand the meaning of scientist/engineer.

The author would also like to express the deepest gratitude to Lecturer Dr. Aya Mizutani Akimoto for her tolerant discussions and warm encouragements. Thanks to her, the author was able to endure the painful tasks, endeavor the continuous researches, and enjoy the life in the laboratory.

The author would like to express his gratitude to Associate Professor Dr. Youn Soo Kim at POSTEC for kindly offering the author the chance of collaboration and giving extensive discussions.

The author would also like to express his gratitude to Professor Dr. Kazuhiko Ishihara, Associate Professor Dr. Yuichi Yamasaki, and Associate Professor Dr. Takamasa Sakai for their extensive discussions and valuable advices.

The author would like to express his gratitude to Dr. Ryota Tamate for his continuous guidance and valuable advices. The author learned a lot of thing from his attitude toward research.

The author would like to express his gratitude to Mr. Kenta Homma and Mr. Michika Onoda for supporting Japan life and valuable advance. The author spent most of his time with them and was able to be smile anytime.

The author appreciates Yoshida-Akimoto Laboratory members: Ms. Catherine Shasteen, Mr. Ryotaro Makita, Mr. Taipei Nishimoto, Ms. Mami Furusawa, Mr Toshiki Yoshizawa, Ms. Ying Gao, Mr. Yi Cui, Mr. Takahiro Otsuka, Mr. Seima Nishimura, and Mr. Komi Sato. Besides, the author would like to thank Yoshida-Akimoto Laboratory past-members.

The author deeply appreciates Japan Society for the Promotion of Science for Young Scientists (JSPS DC1) for the fellowship including research fund during the doctoral course

The author gratefully appreciates his wife, Ms. Hwajin Yang, and his son, Mr. Wooju Lee, for their support and cheer. Thanks to her support and understanding, the author was able to start and finish the doctoral course without any problem. And thank to his son, the author was able to do his best with a sense of responsibility. Therefore, the author promises to be a good husband and a good father.

The author would like to appreciate his parents, Mr. Juha Lee and Ms. Hyunja Lim, and his brother, Mr. Eunkang Lee, for raising and supporting him until now, especially during his long student life for more than 20 years.

In addition, the author would like to appreciate his wife's parents, Mr. Jaeseok Yang and Ms. Eunsoon Lee, and her sister, Ms. Munsuk Yang. Thank to them, the author was able to do his best without worrying about anything. In particular, the author devotes this doctoral dissertation to Mr. Jaeseok Yang and will always remember him.

Finally, when interviewed for admission, the author replied that meaning of doctoral degree is to become an independent researcher. The author will never forget this meaning and carry out it from now.

Eunjong Lee

Department of Materials Engineering

School of Engineering

The University of Tokyo

September 2018

Table of contents

Chapter 1:

General introduction

1-1. Oscillation system by stimuli-responsive polymer hydrogel

Many oscillation systems with rhythm can be observed in organisms[1], such as heartbeat, peristaltic motion within the intestine, brainwaves, the 24-h physiological rhythms, and the annual reproductive cycle of animals and plants, *etc.* These oscillations are sustained during life activities by the spontaneous cyclic reaction in the body, and the oscillation rhythm can be regulated by external stimuli such as temperature and light from surrounding environments.

The polymer hydrogels are cross-linked polymeric 3D-networks swollen in water up to thermodynamic equilibrium[2]. As their physical properties such as high water absorbent and soft elasticity are similar to living tissues, biomedical and pharmaceutical applications of hydrogels have been intensively investigated[3-4].

Beyond these applications, the polymer hydrogels have been applied to representative materials which can mimic oscillation systems. Tanaka *et al*.[5] reported a phenomenon of volume phase transition in the polymer hydrogel composed of poly(acrylamide) (PAAm) by external stimuli such as water/acetone and temperature, as shown in **Figure 1-1**.

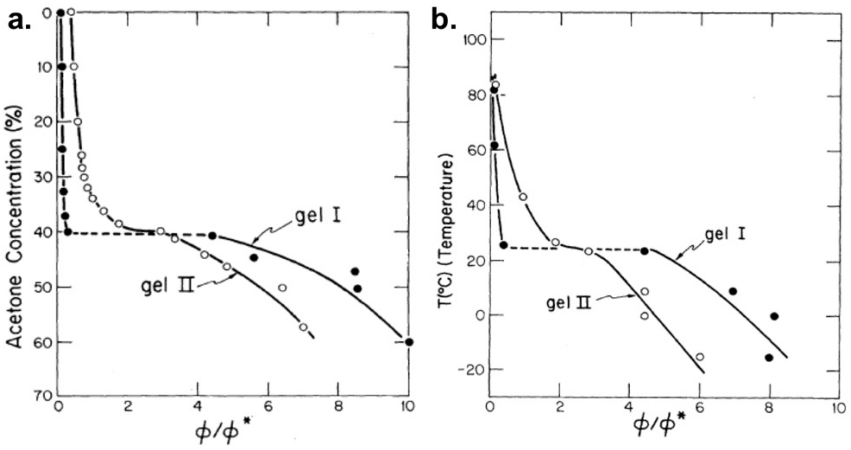

Figure 1-1. The swelling ratio of the poly(acrylamide) gel immersed in water/acetone mixture as a function of **(a)** acetone concentration and **(b)** temperature, respectively[5].

Since the first discovery of volume phase transition by Tanaka *et al.*, the polymer hydrogels, which is responded by various stimuli, have been reported and widely investigated[6-7]: these polymeric materials including polymers and hydrogels are called stimuli-responsive polymeric materials. Stimuli-responsive hydrogels undergo the dynamic oscillation by responding to surroundings[8], such as temperature, pH, light, solvent composition, magnetic and electric field variation, *etc.* Due to dynamic oscillation by their responsiveness, stimuli-responsive hydrogels have been applied to a diverse range of applications, such as shape memory hydrogel[9-11], sensors and biosensors[12], controlled and triggered drug delivery systems[13-16], environmental remediation[17-18], chemo-mechanical soft actuators[19-24], as shown in **Figure 1-2**.

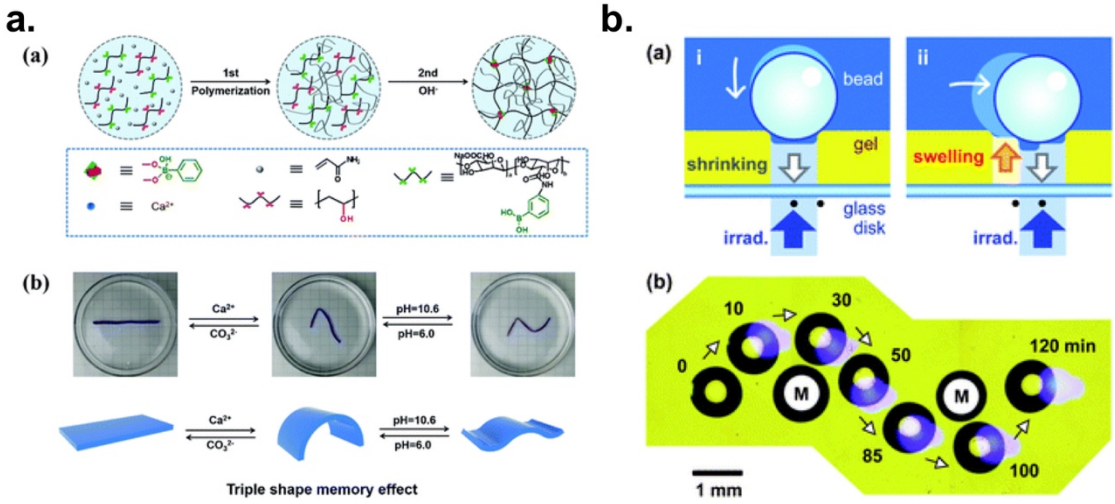

Figure 1-2. Applications of stimuli-responsive hydrogels. **(a)** Shape memory hydrogel using the dual stimuli-responsive hydrogel[11] and **(b)** micro-conveyer system using the photo-responsive hydrogel[24], respectively.

When compared with nature oscillation systems, stimuli-responsive hydrogels require a spontaneous periodic rhythm of stimuli, i.e., on/ off switching of stimuli, to mimic the nature oscillation system driven by a spontaneous cyclic reaction.

1-2. Self-oscillating hydrogel as biomimetic materials

As mentioned in the first paragraph of the previous section, the nature oscillation systems are based on the spontaneous cyclic reaction for the autonomous oscillation, such as heart contraction and breathing. Inspired by nature oscillation system driven by a cyclic reaction, Yoshida *et al.* developed a self-oscillating hydrogel that shows autonomous swelling/deswelling without the on/off switching of external stimuli by employing the Belousov-Zhabotinsky (BZ) reaction[25-29]. The BZ reaction[30], which is a representative model of the nonlinear chemical oscillator, generates a periodic oscillation of chemical species by feedback of different reaction intermediates based on the Field-Körös-Neyes (FKN) mechanism. In 1972, the first FKN mechanism represents temporal oscillations of the BZ reaction. The mechanism consists of 10 elementary reactions, and they can be classified into three groups such as following chemical equations[31-32].

(a) $2Br^- + BrO_3 + 3CH_2(COOH)_2 + 3H^+ \rightarrow 3BrCH(COOH)_2 + 3H_2O$

(b) $BrO_3^- + HBrO_2 + 2M_{Red} \rightarrow 2HBrO_2 + 2M_{Oxi} + H_2O$

(c) $2\ M_{Oxi} + CH_2(COOH)_2 + BrCH(COOH)_2 \rightarrow 2\ M_{Red} + fBr^-$ + other products

Where M_{Red} and M_{Oxi} represent the reduced/oxidized state of metal catalyst participated in the BZ reaction, respectively. However, these chemical equations just represent the total chemical reaction during the BZ reaction, it is difficult to suggest differential equations for understanding the essence of the original process. In 1974, the

FKN mechanism was modified a simple version that generates periodic oscillations: the Oregonator[32]. The Oregonator model represents following 5 reactions that lead to a system of 3 nonlinear differential equations.

$$BrO_3^- + Br^- + 2H^+ \xrightarrow{K_1} HBrO_2 + HOBr \quad (1)$$

$$HBrO_2 + Br^- + H^+ \xrightarrow{K_2} 2HOBr \quad (2)$$

$$BrO3^- + HBrO_2 + H^+ \xrightarrow{K_3} 2HBrO_2 + 2M_{Oxi} \quad (3)$$

$$2HBrO_2 \xrightarrow{K_4} BrO_3^- + HOBr + H^+ \quad (4)$$

$$CH_2(COOH)_2 + M_{Oxi} \xrightarrow{K_5} fBr^- + \text{other products} \quad (5)$$

Where f is a stoichiometric factor; its value has to be in certain rate and is dependent on the concentration of bromate, among other factors. Reactants and product species BrO_3^-, $CH_2(COOH)_2$, and HOBr are generally present in much higher concentrations than the dynamic intermediates Br^-, $HBrO_2$, and oxidized metal-catalyst are assumed to be constant on a time scale of several oscillations. Therefore, the dynamic intermediates can be described by following differential equations.

$$\frac{d[HBrO_2]}{dt} = k_1[BrO_3^-][Br^-][H^+]^2 - k_2[HBrO_2][Br^-][H^+] + k_3[BrO_3^-][HBrO_2][H^+] - 2k_4[HBrO_2]^2$$

$$\frac{d[Br^-]}{dt} = k_1[BrO_3^-][Br^-][H^+]^2 - k_2[HBrO_2][Br^-][H^+] + fk_5[CH_2(COOH)_2][M_{Oxi}]$$

$$\frac{d[M_{Oxi}]}{dt} = k_3[BrO_3^-][HBrO_2][H^+] - fk_5[CH_2(COOH)_2][M_{Oxi}]$$

Based on these differential equations, it is able to understand the relationship between intermediates and to predict oscillation behaviors, as shown in **Figure 1-3**. In particular, the reaction catalyst such as metal ions or metal complexes participate in the cyclic reaction, and they undergo a spontaneous redox oscillation; therefore, the BZ reaction visualizes as color and potential variations.

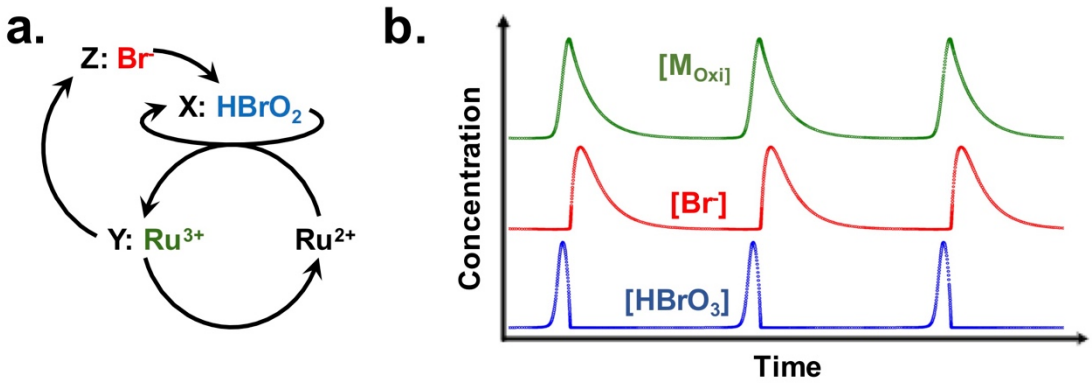

Figure 1-3. **(a)** The relationship between intermediates during the BZ reaction and **(b)** chemical oscillation behaviors of each intermediate, respectively. The oscillation behaviors were simulated by MATLAB.

The self-oscillating hydrogel, which employs the localized BZ reaction within a hydrogel phase, is composed of thermoresponsive polymer, poly(*N*-isoprolacrylamide) (NIPAAm), and ruthenium tris (2,2'-bipyridine) (abbreviated as $Ru(bpy)_3$) covalently bonded to the PNIPAAm network, as shown in **Figure 1-4**. During the course of the BZ reaction, $Ru(bpy)_3$, which is copolymerized with the hydrogel networks and acts as a reaction catalyst, cycles between oxidized and reduced states periodically. Consequently, the self-oscillating hydrogel shows autonomous swelling and deswelling due to increased and decreased hydrohpilicity, respectively[25, 33].

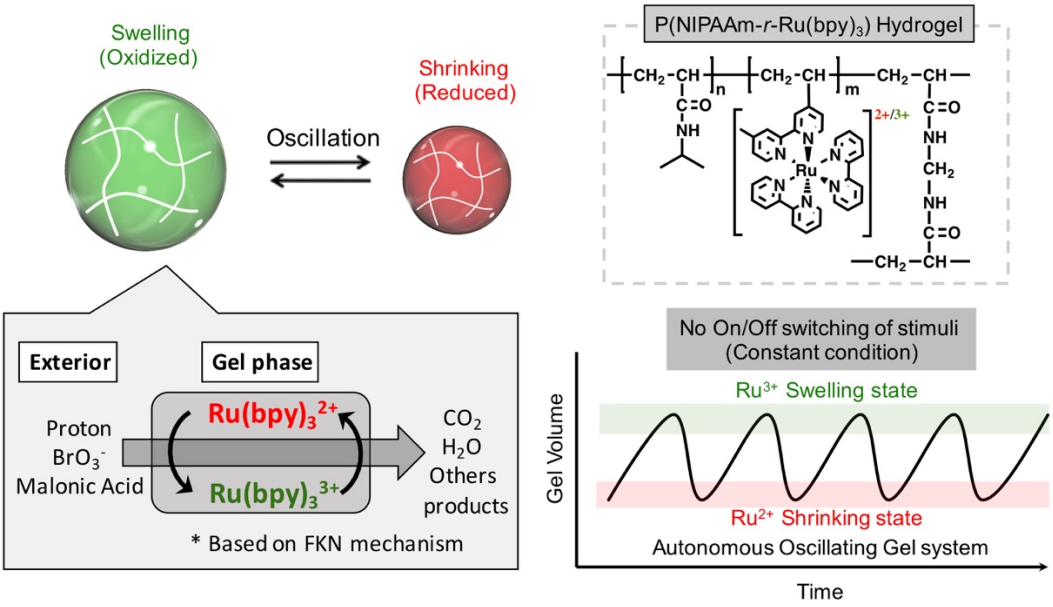

Figure 1-4. the schematic images of the self-oscillating hydrogel driven by the BZ reaction and the chemical structure of the self-oscillating hydrogel.

Furthermore, self-oscillation, which is driven by the BZ reaction, is observed at various scale, from microscopic to macroscopic scale, as shown in **Figure 1-5**. In the case of the linear polymer containing $Ru(bpy)_3$ segments, the polymer solution exhibits self-oscillations of optical transmittance and viscosity due to spontaneous cyclic solubility oscillation of polymers. In case of the self-oscillating hydrogel, it shows autonomous dynamic oscillation driven by the localized BZ reaction; however, the dynamic oscillations represent different aspects depending on the size of hydrogels. The self-oscillating hydrogel with micro-meter size generates entirely synchronized swelling and deswelling like a cardiac muscle cell[34]. However, when the self-oscillating hydrogel is larger than the wavelength of the chemical wave over sub-centimeter length scales, chemical wave propagation with peristaltic motion appears within the hydrogel by coupling with the diffusion of intermediates[35-36].

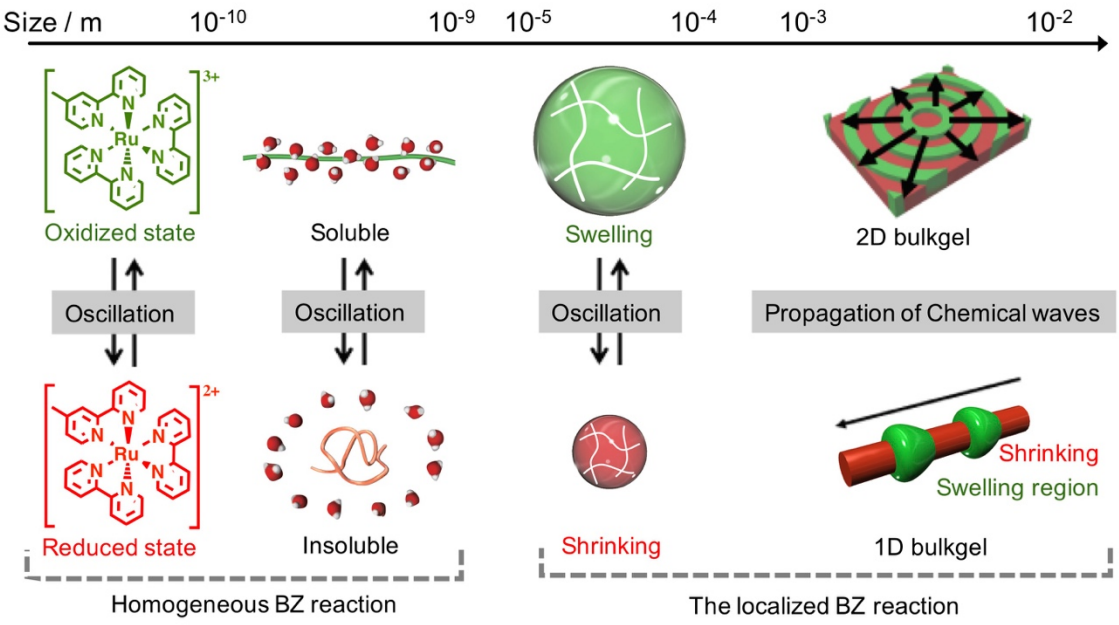

Figure 1-5. Self-oscillation at various scale, from microscopic to macroscopic scale.

1-3. Regulation of dynamic behaviors of self-oscillating hydrogel

The self-oscillating hydrogels have been applied to biomimetic/bioinspired or smart materials by their dynamic behaviors in the two form depending on the size of the self-oscillating hydrogel: (a) the chemical wave propagations with peristaltic motion and (b) the synchronized volume oscillations, respectively.

By using the chemical wave propagation and the following peristaltic motion, autonomous mass transport systems like a conveyer and an intestine have been created [37-40], as shown in **Figure 1-6**. During in course of the BZ reaction, the self-oscillating hydrogel is distinguished between the reduced $Ru(bpy)_3$ regions and the oxidized $Ru(bpy)_3$ regions. These regions move following the propagation direction of the chemical wave due to the diffusion of intermediates. As a result, the object located on or in the self-oscillating hydrogels can be transported by the BZ reaction.

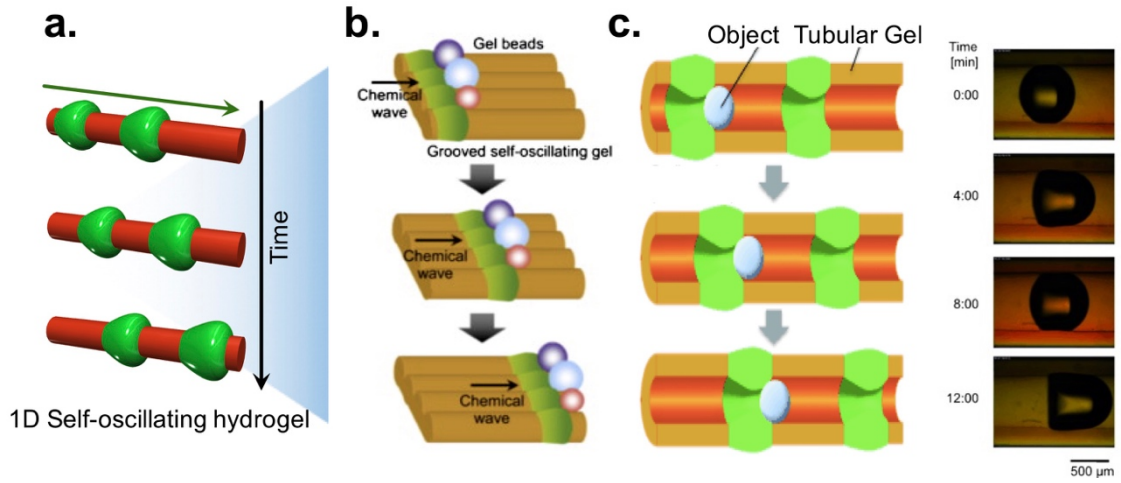

Figure 1-6. (a) The schematic images of the peristaltic motion in the 1D self-oscillating hydrogel. **(b)** the conveyer system consisted of 1D self-oscillating hydrogels[37]. **(c)** the artificial intestine by tubular self-oscillating hydrogel[40], respectively.

However, it is difficult to predict the propagation direction of chemical waves because the propagation directions are based on the probability. The directional control of chemical wave propagation, which determined the operation direction of actuators, is essential to expand as the smart materials. Therefore, the directional control of chemical wave propagation has been developed by various approaches.

Chen *et al.*[41] and Yuan *et al.*[42] demonstrate the directional control of the chemical wave propagation through the variation in the hydrogel shape such as an aspect ratio and polygonal shapes (**Figure 1-7a and b**). In additional, Yuan *et al.*[42] and Masuda *et al.*[43] demonstrate through hydrogels with a gradient structure (**Figure 1-7c**). These hydrogels are prepared by the photo-mask with transparency gradient and the tilted

reaction environment, respectively; therefore, the chemical waves start from the thinner side and propagate the thicker side due to a concentration difference of metal catalysts. Yashin *et al.*[44] fabricates the composite gel systems with a non-active Polyacrylamide gel (PAAm) and the self-oscillating hydrogel patches having different contents (sizes or catalyst concentrations) by the photolithography (**Figure 1-7d**). The chemical waves propagate from small contents to large contents. Moreover, Tateyama *et al*.[45] and Homma *et al*.[46] fabricate the gel array system composed of small self-oscillation patches with the same shapes by the photolithography **(Figure 1-7e)**. The propagation directions are decided by the shape of patches: triangles or pentagons.

The fundamental principle of these approaches is the geometric modification of self-oscillating hydrogels. In order to prepare self-oscillating hydrogels with a controlled propagation direction, therefore, the additional technique such as photolithography is demanded. In addition, the propagation directions are decided from preparation step of self-oscillating hydrogels due to their geometrical structure: it means that they always operate only one way.

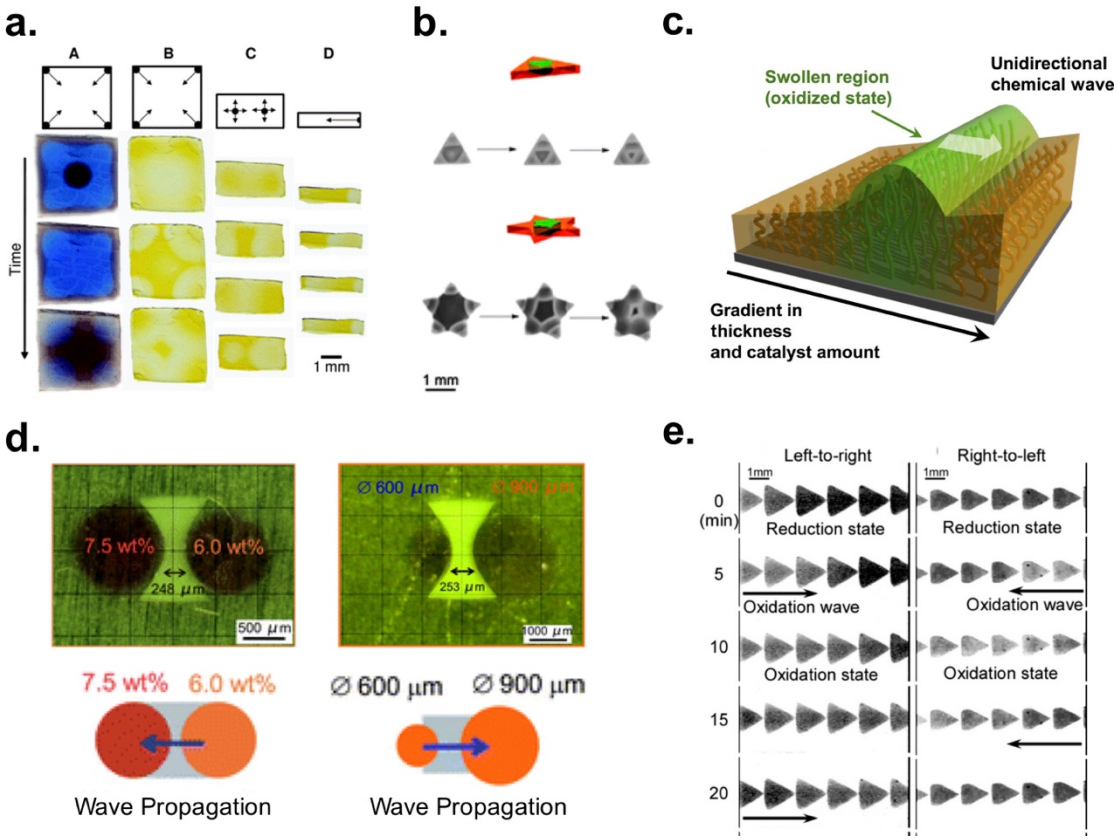

Figure 1-7. The directional control of chemical wave propagation by various approaches. **(a)** the aspect ratio of self-oscillation hydrogel sheet[41], **(b)** the polygonal shape[42], **(c)** the gradient structure[43], **(d)** the composite system consisted of two parts having different contents (Ru catalyst concentration and size)[44], and **(e)** the gel array system composed of small self-oscillation patches[45], respectively.

The self-oscillating hydrogels represent temporal oscillations with a same rhythm during the BZ reaction, and the oscillation rhythm can be regulated by external stimuli, such as temperature change and light, like nature oscillation systems. Beyond the regulation of the oscillation rhythm, the reversible on-off regulation of volume oscillation has been demonstrated by various approaches such as photo-irradiation, the concentration variation of BZ substrates, and temperature change **(Figure 1-8a)**.

Shinohara, *et al*.[47] demonstrates the reversible on-off regulation of volume oscillation by intensity of irradiated light: the photochemical reaction of $Ru(bpy)_3$. When irradiated at a wavelength corresponding metal-to-ligand charge transfer (MLCT) excited state of reduced Ru complexes ($Ru(bpy)_3^{2+}$)[48], the irradiated light generates the excited Ru complexes ($Ru(bpy)_3^{2+*}$). Therefore, the excited Ru complexes, a strong reduction agent, generate two pathways with a reaction intermediate (bromomalonic acid, MABr) and the BZ substrate (bromate, BrO_3^-), and these pathways product an inhibitor (Br^-) and an activator ($HBrO_2$). Although the photochemical reaction generates two competing intermediates, the predominant pathway is the production of an inhibitor, which have been proved by modified Oregonator including two pathways [49] **(Figure 1-8b)**. As a result, the self-oscillation is restricted by the increased concentration of an inhibitor when an intensity of irradiated light increases; the self-oscillation returns to the original state when an intensity of irradiated light decreases.

The BZ reaction can be described by differential equations related to reactants, intermediates, and rate constants. Therefore, the oscillating behaviors changes depending on the concentration of BZ substrate and temperature **(Figure 1-8c)**. Inspired by these characteristics, Yoshida *et al*.[50] demonstrates through a stepwise concentration variation of malonic acid (MA, $CH_2(COOH)_2$); The self-oscillation represents a steady state and an oscillation state depending on the MA concentrations (10 mM and 25 mM), respectively. Moreover, the reversible on-off regulation can be demonstrated by temperature change because of NIPAAm chain in the self-oscillating hydrogel and reaction rate constants of the BZ reaction represented by the differential equation[51].

These approaches show that the reversible on-off regulation of volume oscillation is based on the direct control of the BZ reaction using factors related to kinetics.

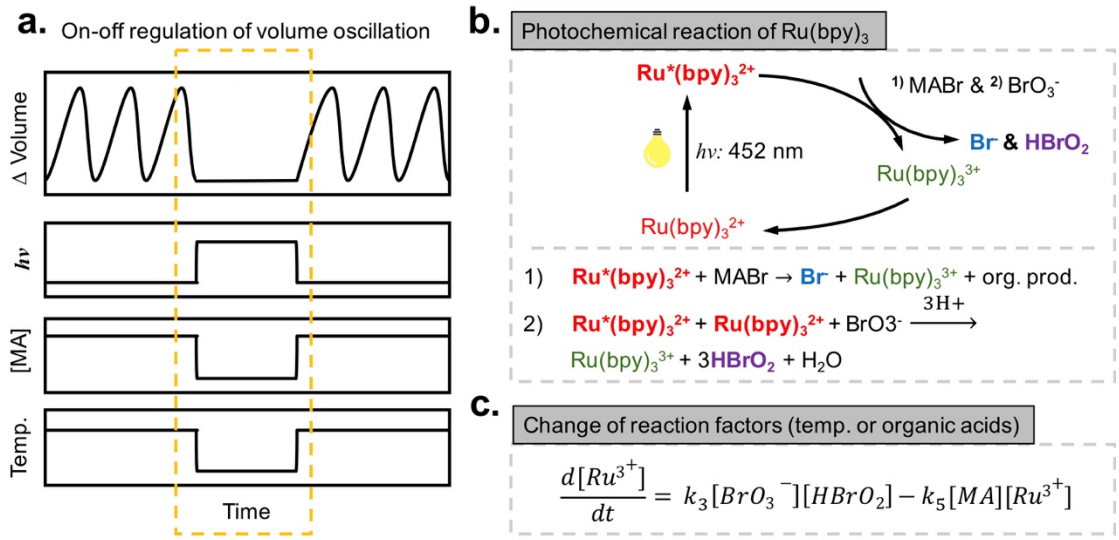

Figure 1-8. The schematic images of **(a)** the reversible on-off regulation of volume oscillation and the detailed mechanism depending on external stimuli: **(b)** irradiated light and **(c)** reaction factors such as organic acid concentration and temperature, respectively.

1-4. Polymer composite materials containing magnetic nanoparticles

Stimuli-responsive hydrogels generate dynamic oscillations by responding to external stimuli, which can deform polymer chain in the form of the expansion or the collapse. Among the responsiveness to various external stimuli, the magnetic responsiveness can provide unique properties (*e.g.,* movement, heat generation) to polymer-based materials, beyond dynamic oscillations. To produce the magnetic responsiveness, the polymer-based materials are contained magnetic nanoparticles.

The polymer composite materials containing magnetic nanoparticles can be classified into three categories according to their activation mode and intended applications, which can be defined by the following aspects (**Figure 1-9**)[52]: (a) The magnetic guidance to move remotely an object to the target area, which has applied in the biomedical application such as cell and molecule guidance and separation. (b) The ability

to be deformed (contraction, deflection, orientation) when exposed to the direct current magnetic field, which has applied in soft actuators and controlled drug release. (c) The heat-generator by the vibration of magnetic nanoparticles within thermoresponsive polymer-based materials when exposed to the alternating magnetic field, which has applied in the controlled drug release and shape memory devices.

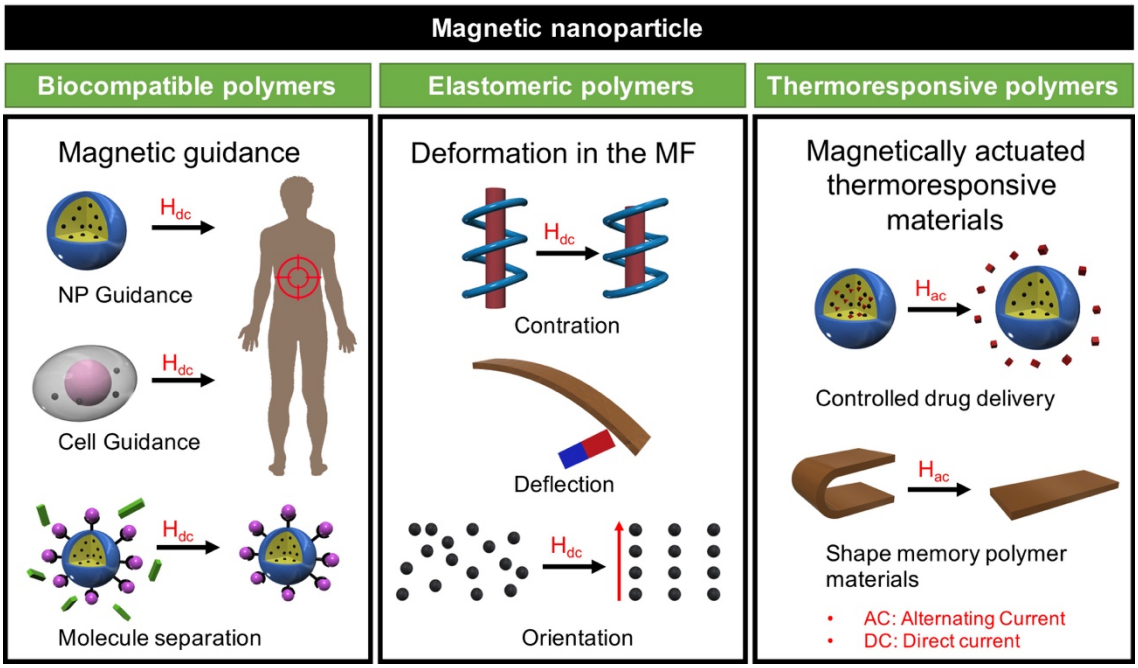

Figure 1-9. The classification of polymer composite materials containing magnetic nanoparticles according to their activation mode and intended applications[52].

The magnetic guidance can provide a precise migration of polymer composite materials containing magnetic nanoparticles according to the migration of the external magnetic field. The polymer composite materials containing magnetic nanoparticles act as a multifunctional structure capable of binding or adsorbing to other species, including for subsequent separation or simple migration.

The conventional drug delivery systems (DDS) are difficult to deliver precisely

to target areas such as cancer or disordered organs within a short time. However, polymer composite materials containing magnetic nanoparticles can provide an excellent tool what the drugs can deliver precisely to target area by an extracorporeal magnetic field while reducing any side effects.

Arias *et al*.[53] demonstrate magnetically driven cancer therapy using squalene-based nanoparticles containing magnetic nanoparticles and the anticancer drug gemcitabine; additionally, it can provide the magnetic resonance imaging (MRI) due to magnetic nanoparticles. The squalene-based nanoparticles, which are guided to the target area by the external magnetic field, are capable of increasing drug accumulation in tumor tissue with subsequent tumor growth inhibition (**Figure 1-10**).

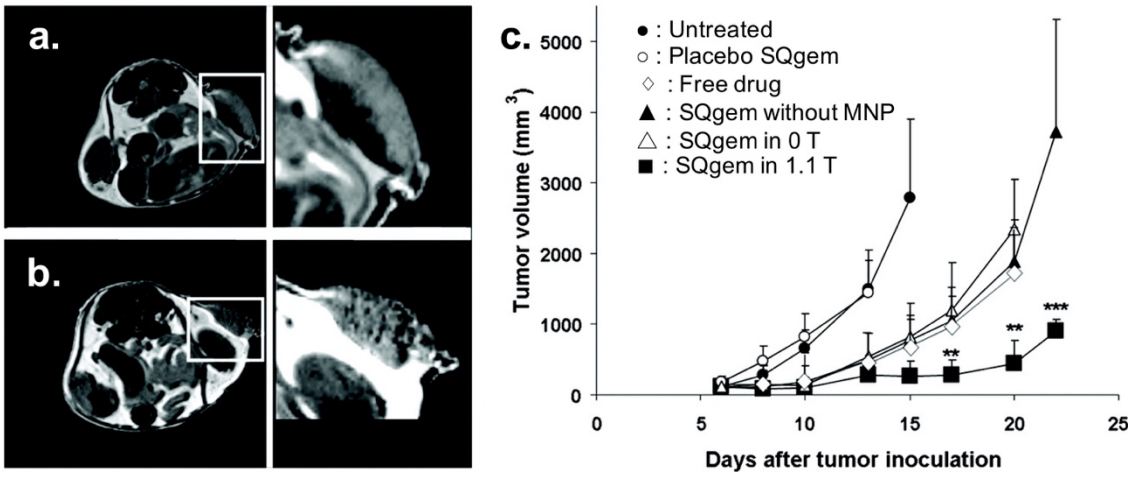

Figure 1-10. The T_2-weighted magnetic resonance images of tumors at 2 h-injection of squalene-based nanoparticles under **(a)** the absence of external field and **(b)** guided by an external magnetic field (1.1 T). **(c)** The in-vivo anticancer activity of squlaene-based nanoparticles comparing the other groups. Where SQgem is squlaene-based nanoparticles containing magnetic nanoparticles and the anticancer drug gemcitabine[53].

In addition, the separation or concentration of certain species in solution has been interested in the biomedical and environmental applications, such as diagnosis systems and contaminant removal systems. These applications are based on the functional polymer brush grafted onto the surface of magnetic nanoparticles[54-56] or the porous structure containing magnetic nanoparticles and functional group[52]; therefore, the target species can bind or absorb with magnetic materials, the separation or concentration are demonstrated by a removal of magnetic materials using the external magnetic field.

The magnetic nanoparticles contained in the hydrogel can be led to an anisotropic deformation of hydrogels by a magnetic cohesion or an orientation of between magnetic nanoparticles, according to the direction of the external magnetic field: this is called the "ferrogel".

Zrinyi *et al*.[57] prepares ferrogel consisted of polyvinyl alcohol (PVA) hydrogel cross-linked by glutaraldehyde and magnetite nanoparticles. And then, they demonstrate a stretching and a contraction of the ferrogel by the localized magnetic field (**Figure 1-11A)**.

Since then, Zhao *et al*.[58] demonstrate the drug release by the macro-porous ferrogel consisted of RGD-modified alginate hydrogel cross-linked with adipic acid dihydrazide (AAD), and Pluronic F127 coated magnetic nanoparticles for a homogeneous dispersion. The macro-porous structure is prepared by the lyophilization, and the porous size is determined by freezing temperature. when compared with nano-porous structure, the macro-porous structure shows a reversible and larger deformation by the magnetic field (**Figure 1-11B)**. In addition, the controlled release of various drugs is demonstrated by the reversible magnetic deformation, as shown in **Figure 1-11C**.

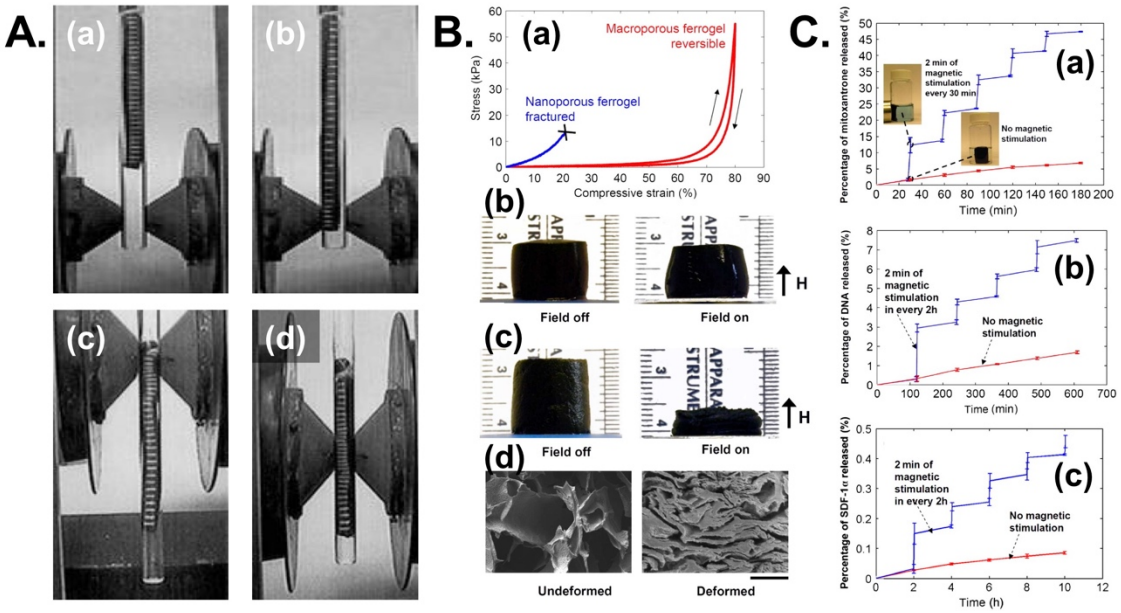

Figure 1-11. **A)** The stretching and a contraction of the ferrogel by the localized magnetic field. (a) no magnetic field; The maximal field strength is located (b) under the low end of the ferrogel, (b) on the top surface of the ferrogel, and (c) in the middle of the hydrogel, respectively.[57] **B)** Porous ferrogels with a volume deformation by magnetic field. **C)** Cumulative release profiles of drugs from macroporous ferrogels subject to 2min of magnetic stimulation every 2 h or no-magnetic stimulation[58].

The magnetic nanoparticles generate heat by their vibration under the alternating magnetic field: it means that the temperature change can be remotely controlled. Therefore, the magnetic nanoparticles can provide a programmed response when they are introduced into the thermoresponsive polymer based materials and this system has been demonstrated primarily in two areas: DDS[59-62] and shape memory devices[63-65].

As a result, the polymer composite materials containing magnetic nanoparticles can provide additional unique properties as mentioned above. Although these have been primarily applied in the biomedical field, are expected to expand into diverse applications by combining with various polymer-based materials.

1-5. Scope of this research

The nature oscillation systems are driven by a spontaneous cyclic reaction, and the oscillation rhythms can be regulated by external stimuli. Inspired by nature oscillation systems, self-oscillating hydrogels have been developed and applied to biomimetic/ bioinspired soft materials due to an autonomous BZ reaction. However, self-oscillating hydrogels are facing the problem of the regulation of self-oscillation that appears in the form of the volume oscillation and chemical wave propagation to control various motions beyond a simple motion. For past few decades, the regulation methods of dynamic behaviors in self-oscillating hydrogels are based on the geometric modification of self-oscillation hydrogels having a fixed directionality from the initial state and the direct control of the BZ reaction related in the spontaneous cyclic reaction, respectively.

The general structure of self-oscillating hydrogels is composed of PNIAAm and Ru catalysts, and each segment related to temperature, and redox oscillation which occurs in a strongly acidic condition, respectively. Except for these two stimuli, the author investigated a proper property which can be introduced into the self-oscillating hydrogel without affecting the BZ reaction. Among the many properties, which can provide a new function to self-oscillating hydrogels, the magnetic property is suitable for this research object because it can offer the following unique capabilities: (a) the remote control without affecting the mechanism of the BZ reaction (b) the ability to migrate target object precisely where desired, and (c) the anisotropic deformation by the magnetic field.

The final goal of the doctoral dissertation is the regulation of dynamic behaviors, which appeared in the form of a chemical wave propagation and a volume oscillation depending on the size of hydrogels, by the magnetic field. In order to achieve this goal, the magnetic nanoparticles were introduced into self-oscillating hydrogels, and dynamic behaviors were regulated by magnetic activation modes, as shown in the **Figure 1-12**.

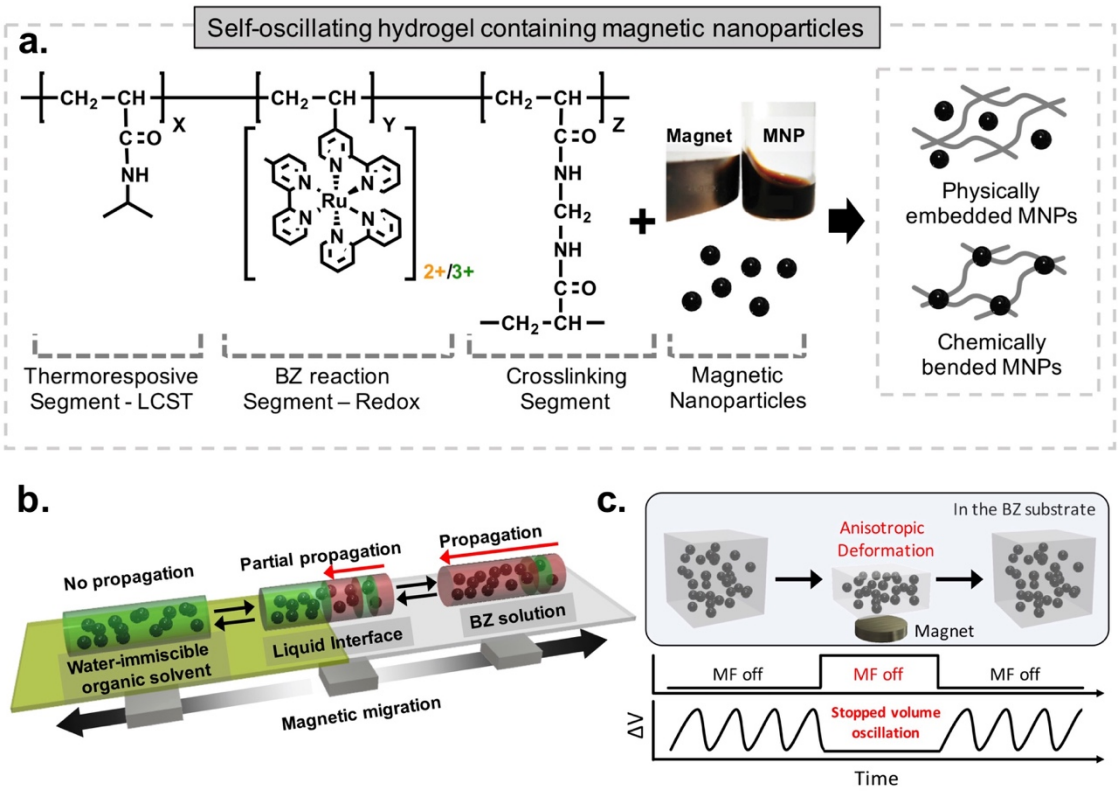

Figure 1-12. Overview of this dissertation. **(a)** Development of self-oscillating hydrogels containing magnetic nanoparticles (Chapter 2), **(b)** the directional control of chemical wave propagation by the magnetic migration (Chapter 3), and **(c)** the reversible on-off regulation of volume oscillation in the self-oscillating hydrogel by the magnetic deformation (Chapter 4), respectively.

In chapter 2., the synthetic strategy of self-oscillating hydrogels containing magnetic nanoparticles is investigated. Self-oscillating hydrogels containing magnetic nanoparticles are prepared by different methods depending on the binding methods between magnetic nanoparticles and hydrogel network such as (1) physically embedded magnetic nanoparticles and (2) chemically bonded magnetic nanoparticles respectively.

In chapter 3., the directional control of chemical wave propagations is demonstrated by magnetic migrations of self-oscillating hydrogels physically containing

magnetic nanoparticles in liquid-liquid layers. Moreover, the reversible propagation of chemical waves in the same hydrogel phase is demonstrated by the continuous position modulation in the three-layers system consisted of aqueous BZ solution and water immiscible organic solvents (hexane and dichloromethane).

In chapter 4., the reversible on-off regulation of the volume oscillation in self-oscillating hydrogels by the magnetic deformation is investigated. The external magnetic field can lead to the network deformation of hydrogels containing magnetic nanoparticles, and the deformation degree can be controlled by their pore size. In order to induce a large magnetic deformation of self-oscillating hydrogels by the external magnetic field, the bulk-gel with porous structure is fabricated by the linked self-oscillating hydrogel beads chemically containing magnetic nanoparticles. Thus, the reversible on-off regulation of volume oscillation is demonstrated by magnetic deformation, which occurs by applying the reversible magnetic field.

Finally, in Chapter 5, the researched in this dissertation are summarized, and future perspectives about self-oscillating hydrogels containing magnetic nanoparticles applicable to the energy conversion system are described.

1-6. References

[1] K. Uriu, *Development, growth & differentiation* **2016**, *58*, 16.

[2] M. C. Koetting, J. T. Peters, S. D. Steichen, N. A. Peppas, *Materials Science and Engineering: R: Reports* **2015**, *93*, 1.

[3] J. Malda, J. Visser, F. P. Melchels, T. Jüngst, W. E. Hennink, W. J. Dhert, J. Groll, D. W. Hutmacher, *Adv. Mater.* **2013**, *25*, 5011.

[4] N. Annabi, A. Tamayol, J. A. Uquillas, M. Akbari, L. E. Bertassoni, C. Cha, G. Camci-Unal, M. R. Dokmeci, N. A. Peppas, A. Khademhosseini, *Adv. Mater.* **2014**, *26*, 85.

[5] T. Tanaka, *Phys. Rev. Lett.* **1978**, *40*, 820.

[6] L. Zhai, *Chem. Soc. Rev.* **2013**, *42*, 7148.

[7] A. Khan, J. Pessin, *Diabetologia* **2002**, *45*, 1475.

[8] R. Yoshida, T. Okano, in *Biomedical applications of hydrogels handbook*, Springer, **2010**, pp. 19.

[9] Y. Osada, A. Matsuda, *Nature* **1995**, *376*, 219.

[10] H. Meng, P. Xiao, J. Gu, X. Wen, J. Xu, C. Zhao, J. Zhang, T. Chen, *Chem. Commun.* **2014**, *50*, 12277.

[11] X. Le, W. Lu, J. Zheng, D. Tong, N. Zhao, C. Ma, H. Xiao, J. Zhang, Y. Huang, T. Chen, *Chemical science* **2016**, *7*, 6715.

[12] J. Hu, S. Liu, *Macromolecules* **2010**, *43*, 8315.

[13] N. Peppas, P. Bures, W. Leobandung, H. Ichikawa, *Eur. J. Pharm. Biopharm.* **2000**, *50*, 27.

[14] S. J. Jhaveri, M. R. Hynd, N. Dowell-Mesfin, J. N. Turner, W. Shain, C. K. Ober, *Biomacromolecules* **2008**, *10*, 174.

[15] A. S. Hoffman, *J. Controlled Release* **2008**, *132*, 153.

[16] A. Bajpai, S. K. Shukla, S. Bhanu, S. Kankane, *Prog. Polym. Sci.* **2008**, *33*, 1088.

[17] D. Parasuraman, M. J. Serpe, *ACS Appl. Mater. Interfaces* **2011**, *3*, 2732.

[18] D. Parasuraman, M. J. Serpe, *ACS Appl. Mater. Interfaces* **2011**, *3*, 4714.

[19] Y. Osada, H. Okuzaki, H. Hori, *Nature* **1992**, *355*, 242.

[20] R. Yoshida, K. Uchida, Y. Kaneko, K. Sakai, A. Kikuchi, Y. Sakurai, T. Okano, *Nature* **1995**, *374*, 240.

[21] M. Ma, L. Guo, D. G. Anderson, R. Langer, *Science* **2013**, *339*, 186.

[22] Y. Osada, J. P. Gong, *Adv. Mater.* **1998**, *10*, 827.

[23] A. Richter, S. Klatt, G. Paschew, C. Klenke, *Lab on a Chip* **2009**, *9*, 613.

[24] T. Satoh, K. Sumaru, T. Takagi, T. Kanamori, *Soft Matter* **2011**, *7*, 8030.

[25] R. Yoshida, T. Takahashi, T. Yamaguchi, H. Ichijo, *J. Am. Chem. Soc.* **1996**, *118*, 5134.

[26] R. Yoshida, T. Ueki, *NPG Asia Materials* **2014**, *6*, e107.

[27] R. Tamate, T. Ueki, R. Yoshida, *Adv. Mater.* **2015**, *27*, 837.

[28] R. Tamate, T. Ueki, R. Yoshida, *Angew. Chem. Int. Ed.* **2016**, *55*, 5179.

[29] Y. S. Kim, R. Tamate, A. M. Akimoto, R. Yoshida, *Materials Horizons* **2017**, *4*, 38.

[30] A. Zaikin, A. Zhabotinsky, *Nature* **1970**, *225*, 535.

[31] R. M. Noyes, R. Field, E. Koros, *J. Am. Chem. Soc.* **1972**, *94*, 1394.

[32] R. J. Field, E. Koros, R. M. Noyes, *J. Am. Chem. Soc.* **1972**, *94*, 8649.

[33] R. Yoshida, E. Kokufuta, T. Yamaguchi, *Chaos: An Interdisciplinary Journal of Nonlinear Science* **1999**, *9*, 260.

[34] R. Yoshida, M. Tanaka, S. Onodera, T. Yamaguchi, E. Kokufuta, *J. Phys. Chem. A* **2000**, *104*, 7549.

[35] Y. Takeoka, M. Watanabe, R. Yoshida, *J. Am. Chem. Soc.* **2003**, *125*, 13320.

[36] S. Sasaki, S. Koga, R. Yoshida, T. Yamaguchi, *Langmuir* **2003**, *19*, 5595.

[37] Y. Murase, M. Hidaka, R. Yoshida, *Sensors Actuators B: Chem.* **2010**, *149*, 272.

[38] S. Maeda, Y. Hara, R. Yoshida, S. Hashimoto, *Angew. Chem.* **2008**, *120*, 6792.

[39] Y. Murase, S. Maeda, S. Hashimoto, R. Yoshida, *Langmuir* **2008**, *25*, 483.

[40] Y. Shiraki, R. Yoshida, *Angew. Chem. Int. Ed.* **2012**, *51*, 6112.

[41] I. C. Chen, O. Kuksenok, V. V. Yashin, R. M. Moslin, A. C. Balazs, K. J. Van Vliet, *Soft Matter* **2011**, *7*, 3141.

[42] P. Yuan, O. Kuksenok, D. E. Gross, A. C. Balazs, J. S. Moore, R. G. Nuzzo, *Soft Matter* **2013**, *9*, 1231.

[43] T. Masuda, A. M. Akimoto, K. Nagase, T. Okano, R. Yoshida, *Science advances* **2016**, *2*, e1600902.

[44] V. V. Yashin, S. Suzuki, R. Yoshida, A. C. Balazs, *J. Mater. Chem.* **2012**, *22*, 13625.

[45] S. Tateyama, Y. Shibuta, R. Yoshida, *Journal of Physical Chemistry B* **2008**, *112*, 1777.

[46] K. Homma, T. Masuda, A. M. Akimoto, K. Nagase, K. Itoga, T. Okano, R. Yoshida, *Small* **2017**, *13*.

[47] S. i. Shinohara, T. Seki, T. Sakai, R. Yoshida, Y. Takeoka, *Angew. Chem.* **2008**, *120*, 9179.

[48] D. W. Thompson, A. Ito, T. J. Meyer, *Pure Appl. Chem.* **2013**, *85*, 1257.

[49] S. Kádár, T. Amemiya, K. Showalter, *J. Phys. Chem. A* **1997**, *101*, 8200.

[50] R. Yoshida, K. Takei, T. Yamaguchi, *Macromolecules* **2003**, *36*, 1759.

[51] R. Yoshida, *Polym. J.* **2010**, *42*, 777.

[52] J. Thévenot, H. Oliveira, O. Sandre, S. Lecommandoux, *Chem. Soc. Rev.* **2013**, *42*, 7099.

[53] J. L. Arias, L. H. Reddy, M. Othman, B. Gillet, D. Desmaële, F. Zouhiri, F. Dosio, R. Gref, P. Couvreur, *ACS Nano* **2011**, *5*, 1513.

[54] F. Xu, J. H. Geiger, G. L. Baker, M. L. Bruening, *Langmuir* **2011**, *27*, 3106.

[55] J. J. Lai, K. E. Nelson, M. A. Nash, A. S. Hoffman, P. Yager, P. S. Stayton, *Lab on a Chip* **2009**, *9*, 1997.

[56] A. C. Anaïs, B. Stefano, D. Stéphanie, V. Jean-Louis, M. Laurent, *Angew. Chem. Int. Ed.* **2012**, *51*, 10765.

[57] M. Zrínyi, L. Barsi, A. Büki, *J. Chem. Phys.* **1996**, *104*, 8750.

[58] X. Zhao, J. Kim, C. A. Cezar, N. Huebsch, K. Lee, K. Bouhadir, D. J. Mooney, *PNAS* **2011**, *108*, 67.

[59] S. Louguet, B. Rousseau, R. Epherre, N. Guidolin, G. Goglio, S. Mornet, E. Duguet, S. Lecommandoux, C. Schatz, *Polymer Chemistry* **2012**, *3*, 1408.

[60] H. Shang-Hsiu, L. Bang-Jie, C. Chin-Sheng, C. Po-Jung, C. I-Wei, C. San-Yuan, *Adv. Mater.* **2012**, *24*, 3627.

[61] S.-H. Hu, S.-Y. Chen, X. Gao, *ACS Nano* **2012**, *6*, 2558.

[62] C. Wei-Lun, K. Cherng-Jyh, L. Zi-Xian, C. San-Yuan, C. Fu-Rong, T. Chun-Ying, X. Younan, S. Hsing-Wen, *Small* **2012**, *8*, 3584.

[63] U. N. Kumar, K. Kratz, W. Wagermaier, M. Behl, A. Lendlein, *J. Mater. Chem.* **2010**, *20*, 3404.

[64] K. U. Narendra, K. Karl, H. Matthias, B. Marc, L. Andreas, *Adv. Mater.* **2011**, *23*, 4157.

[65] M. Y. Razzaq, M. Behl, A. Lendlein, *Adv. Funct. Mater.* **2012**, *22*, 184.

Chapter 2:

Development of self-oscillating hydrogel containing magnetic nanoparticles

2-1. Introduction

Magnetic hydrogels have been achieved by the introduction of magnetic nanoparticles, which can quickly respond to the external magnetic filed and enable their enhanced controllability[1-5], into the hydrogel networks. Therefore, magnetic hydrogels, i.e., hydrogels containing magnetic nanoparticles, have been prepared by various methods that distinguished by the binding types between magnetic nanoparticles and the hydrogel networks: physically embedded magnetic nanoparticles and chemically bonded magnetic nanoparticles, respectively. The preparation methods are classified by Li *et al*[6], such as (a) the blending method, (b) the *in situ* precipitation method, and (c) the grafting-onto method, as shown in **Figure 2-1**[6]. In this classification, the magnetic hydrogels, which are prepared by the blending method and the *in situ* precipitation method, have physically embedded magnetic nanoparticles. In addition, the chemically bonded magnetic nanoparticles within hydrogel networks is achieved by the grafting onto method.

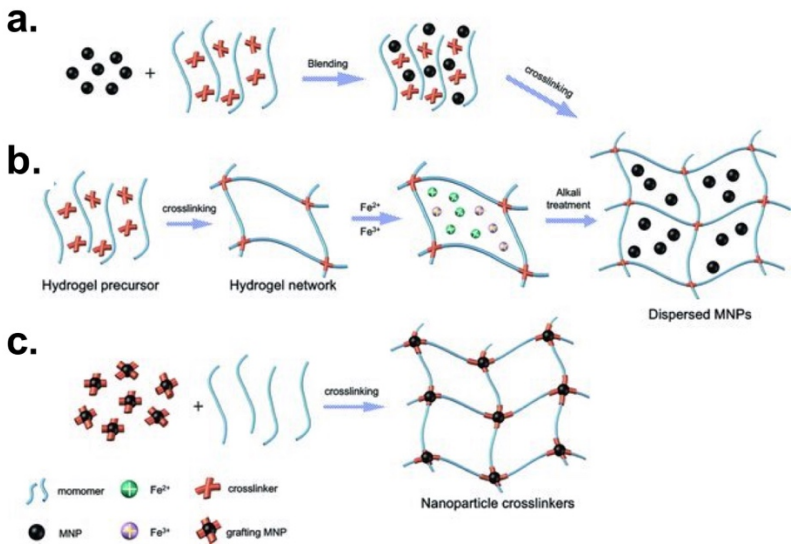

Figure 2-1. Schematic of preparation methods of magnetic hydrogels. **(a)** the blending method, **(b)** the in situ precipitation method, and **(c)** grafting-onto method, respectively[6].

The blending method is based on the crosslinking between monomers and cross-linkers; thus, the magnetic nanoparticles, which are provided as a suspension, are encapsulated within hydrogel phase. Therefore, it can control the concentration of magnetic nanoparticles in the hydrogel phase by the suspension concentration. However, it is difficult to obtain a uniform distribution of magnetic nanoparticles within the hydrogel networks, and magnetic nanoparticles can diffuse out of the hydrogel phase because they are just embedded in hydrogel networks.

The *in situ* precipitation method is achieved by following process. First, the hydrogel is prepared and immersed in the concentrated aqueous solution containing Fe^{2+} and Fe^{3+} (molar ratio of 1:2) until a swelling equilibrium is reached. And then, the hydrogel containing ferrous ions is transferred into precipitating agents solution[7-8] (e.g., NaOH, $NH_3 \cdot H_2O$) to reduce magnetic nanoparticles. Finally, the magnetic nanoparticles are physically located in the hydrogel phase. The *in situ* precipitation can introduce large number of magnetic nanoparticles into the hydrogel. However, it is only suitable for specific hydrogel networks because the precipitating agent can destroy them[9].

The magnetic hydrogels prepared by above two methods have no covalent bond between magnetic nanoparticles and hydrogel networks; therefore, the stability of magnetic nanoparticles and hydrogel networks is not guaranteed[10]. While the external magnetic field induces a magnetic dipole of magnetic nanoparticles, the interaction of between magnetic nanoparticles occurs when they are close enough to affect their neighbors. Therefore, The magnetic nanoparticles are aligned in an end-to-end configuration by the attraction with each other, and thus a "pearl-chain structure" is built *via* the attractive force (**Figure 2-2a**)[11]. Therefore, the magnetic nanoparticles undergo movements for aligning and cohesion along the direction of the magnetic field, and these actions can destroy the hydrogel networks. Furthermore, when the external magnetic field

is applied in the state where magnetic nanoparticles are irregularly located in the hydrogel, the actions of magnetic nanoparticles divides the hydrogel networks into the contracted and stretched regions; thus, the destroyed networks can observe in the stretched region (**Figure 2-2b**)[12]. Besides, the applying the reversible magnetic field can increase the damage of hydrogel networks, based on these mechanisms.

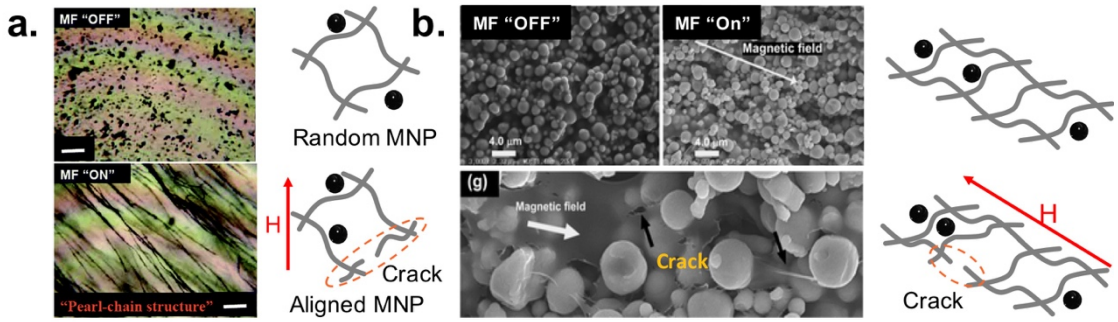

Figure 2-2. the destruction mechanisms of the hydrogel network by magnetic motions. **(a)** the aligned magnetic nanoparticles[11] and **(b)** the irregular distribution of magnetic nanoparticles[12], respectively.

The preparation method of magnetic hydrogel achieved by the covalent bond between magnetic nanoparticles and hydrogel networks, called the grafting-onto method. In order to bind covalently with monomers and magnetic nanoparticles, the surface of magnetic nanoparticles is modified by functional groups such as primary amine[4] and methacrylic groups[13]. Therefore, the magnetic nanoparticles can be trapped in the hydrogel networks without seeping out, by the covalent bond or conjugation. Besides, the chemical arrangement of magnetic nanoparticles can prevent the damage to magnetic motion because the polymer chain bound to magnetic nanoparticles are "roll-up" instead of the linear movement by the direction of the magnetic nanoparticles[14]. The magnetic hydrogel prepared by the grafting-onto method provide a good solution about the stability

of magnetic nanoparticles and hydrogel networks. In case of vinyl functionalized magnetic nanoparticles, however, it can create not only cross-linking points but also magnetic nanoparticles chain. Therefore, it is difficult to introduce a high concentration of magnetic nanoparticles in the hydrogel phase.

In this study, the preparation methods of self-oscillating hydrogels containing magnetic nanoparticles were investigated. The conventional self-oscillating hydrogels have been prepared by following methods: (a) the direct-gelation based on the free radical polymerization with monomers and low molecular cross-linkers. (b) The post-conjugation of $Ru(bpy)_3$ in the hydrogel phase, which has primary amine groups. However, it is difficult not only to measure a concentration of Ru contents in the self-oscillating hydrogels but also to introduce magnetic nanoparticles into the self-oscillating hydrogel phase due to the rapid sedimentation of magnetic nanoparticles during the gelation. Therefore, the author designed a new approach to prepare the self-oscillating hydrogel containing magnetic nanoparticles to overcome these drawbacks, and it was achieved by functional copolymers and surface modified magnetic nanoparticles.

2-2. Experiments section

2-2-1. Materials

N-isopropylacrylaminde (NIPAAm) was kindly provided by Kojin (Japan) and purified by recrystallization in toluene/n-hexane. *N*-(3-Aminopropyl) methacrylamide hydrochloride (NAPMAm) was purchased from Polyscience (USA) and used as received. Two-types of magnetic nanoparticles (hard ferrite and soft ferrate) were kindly provided Powdertech (Japan) and used as received. The average particle size of these magnetic nanoparticles is 100 nm; the detail magnetic properties and density are summarized in **Table 2-1**. 2,2'-azobis (isobutyronitrile) (AIBN) was purchased from Wako Pure

Chemical Industries (Japan) and was purified by recrystallization from methanol. Bis (2,2'-bipyridine) (1-(4'-methyl-2,2'-bipyridine-4-carbonyloxy)-2,5-pyrrolidinedione) ruthenium(II) bis (hexafluorophosphate)(abbreviated as $Ru(bpy)_3$-NHS) was synthesized according to the previous report.[15] The chain transfer agent, S-1-dodecyl- S'-(*α*, *α*'-dimethyl- *α*''-acetic acid)-trithiocarbonate (DDMAT, purify >99 %), was purchased from Trylead Chemical Technology (China) and used as received. *N*-Acryloxysuccinimide (NAS) and glutaraldehyde (50% solution, 5.6 mol/L) were purchased from Tokyo Kasei (Japan) and used as received. *N*, *N*-Dimethylacrylamide (DMAAm) was purchased from Wako Pure Chemical Industries (Japan) and used as received. (3-Aminopropyl)-triehoxylsilane (APTES) was purchased from Sigma Aldrich and used as received. *N,N'*-methylenebisacrylamide (MBAAm) was purchased form Acros Organics (Geel, Belgium) and used as received. *N,N,N',N'*-tetramehtylethylendiamine (TEMED) and ammonium peroxide (APS) were purchased from Wako Pure Chemical Industries (Japan) and used as received. All other chemicals were purchased from Wako Pure Chemical Industries (Japan) and used as received.

Table 2-1. The detail magnetic properties of magnetic nanoparticles depending on the ferrite types. the magnetic properties were measured at 5 K. The hard ferrite composed of only $SrO•6Fe_2O_3$ and soft ferrite composed of $(FeO,MnO,MgO)•Fe_2O_3$ and $SrO•6Fe_2O_3$, respectively.

	Saturated Magnetization(M_s)	Remnant Magnetization(M_r)	coercitivity (H_c)	Density (g/cm^3)
Hard ferrite	48 emu/g	26 emu/g	1500 Oe	4.75
Soft ferrite	55 emu/g	9 emu/g	75 Oe	4.85

2-2-2. Synthesis and characterization of *P(NIPAAm-r-NAPMAmRu(bpy)$_3$-r-NAPMAm) copolymer*

The P(NIPAAm-*r*-NAPAAmRu(bpy)$_3$-*r*-NAPMAm) was prepared by reversible addition−fragmentation chain-transfer (RAFT) random copolymerization (**Figure 2-3a**) as previously reported[16]. Briefly, DDMAT (182 mg, 0.5 mmol), NIPAAm (7.91 g, 70 mmol) and NAPAAm (890 mg, 5 mmol) were dissolved in the 45mL of methanol. A solution of AIBN (8.2 mg, 0.05 mmol) in the 5 ml of methanol) was added to the monomer solution, and the mixture was bubbled with Ar for 20 min. The RAFT random copolymerization was then carried out at 60 °C for 16 hours. After the reaction, the solvent was removed by evaporation. The product was dissolved in the 50 mL of acetone and was purified by reprecipitation from acetone/n-hexane as good/poor solvents and then dried under vacuum at room temperature. The prepared copolymer, P(NIPAAm-*r*-NAPMAm), included dodecyl trithoiocarbonate residue parts derived from the DDMAT. To exchange from the residue parts to CN group, the dried copolymer was dissolved in 200 mL of ethanol. The solution of AIBN (30 times mol of a dissolved copolymer) in the 150 mL of ethanol was added to the copolymer solution, and the mixture was bubbled with Ar for 20 min. The reaction was then carried out at 80 °C for 16 hours. The product was concentrated by evaporation and was purified by reprecipitation from *n*-hexane and then dried under vacuum at room temperature.

Next, the Ru(bpy)$_3$-NHS was introduced into P(NIPAAm-*r*-NAPMAm) copolymer (**Figure 2-3b**). The prepared copolymer (395 mg, 0.025 mmol) was dissolved in 15 mL of DMSO. 5 ml of DMSO with Ru(bpy)$_3$-NHS (110 mg, 0.11mmol) and Triethylamine (TEA, 0.21 mL, 1.5 mmol) was mixed into the copolymer solution and the solution was stirred at room temperature for 3 hours. The products were purified by

dialysis against D.I water for 2 days and then freeze-dried. Finally, the P(NIPAAm-*r*-NAPMAmRu(bpy)$_3$-*r*-NAPMAm) was obtained. The Ru(bpy)$_3$ content in the copolymer was determined by a UV-vis spectroscopy (UV-2500 PC, Shimadzu). The introduced amount of Ru(bpy)$_3$ was calculated by using a calibration curve (**Figure 2-4**) measured by absorption values at 465 nm depending on the concentration of Ru(bpy)$_3$Cl$_2$. [3] The ^{1}H-NMR measurement was conducted to characterize and to confirm the composition of the copolymer. The measurement was performed in D_2O with a JEOL ECS 400 (400 MHz) at room temperature. The number-averaged-molecular weight of PNIPAAm and PNAPMAm of the copolymer were calculated using the ratio of integrated signal intensities for the characteristic isopropyl group of PNIPAAm (1H, δ = 3.81 ppm) and the characteristic propyl group of PNAPMAm (4H, δ = 2.85 – 3.27 ppm). The conjugated Ru(bpy)$_3$ in copolymer chain was confirmed by signal of methyl group (3H, δ = 2.6 ppm) and bipyridine group of Ru(bpy)$_3$ (6H, δ = 7.3 – 7.5 ppm) (9H, δ = 7.8 – 8.2 ppm), (7H, δ = 8.6 – 8.9 ppm) (**Figure 2-5**), respectively. The polydispersity index (PDI; Mw/Mn) of the copolymer was measured by a GPC system (Tosoh, Japan), using DMF containing 50 mM LiCl as the mobile agent. The GPC columns were calibrated by using a PEO standards.

2-2-3. *Synthesis of P(DMAAm-r-NAS) linear polymer*

The P(DMAAm-*r*-NAS) was prepared by the free radical random polymerization (**Figure 2-3c**) as previously reported[17]. Briefly, DMAAm (4.55 mL, 44.2 mmol) and NAS (0.37 g, 2.21 mmol) were dissolved in the 24 mL of 1,4 dioxane. A solution of AIBN (36.3 mg, 0.22 mmol in the 6 mL of 1,4 dioxane) was added to monomer solution, and the mixed solution was bubbled with Ar for 20 min. The free radical polymerization was then carried out at 65 °C for 1 day. After the reaction, the solvent was removed by

evaporation. The product was dissolved in the 30 mL of acetone and was purified by reprecipitation from acetone/n-hexane as good/poor solvents and then dried under vacuum at room temperature. The final product was stored at 0 °C of the refrigerator to prevent a decomposition of NAS.

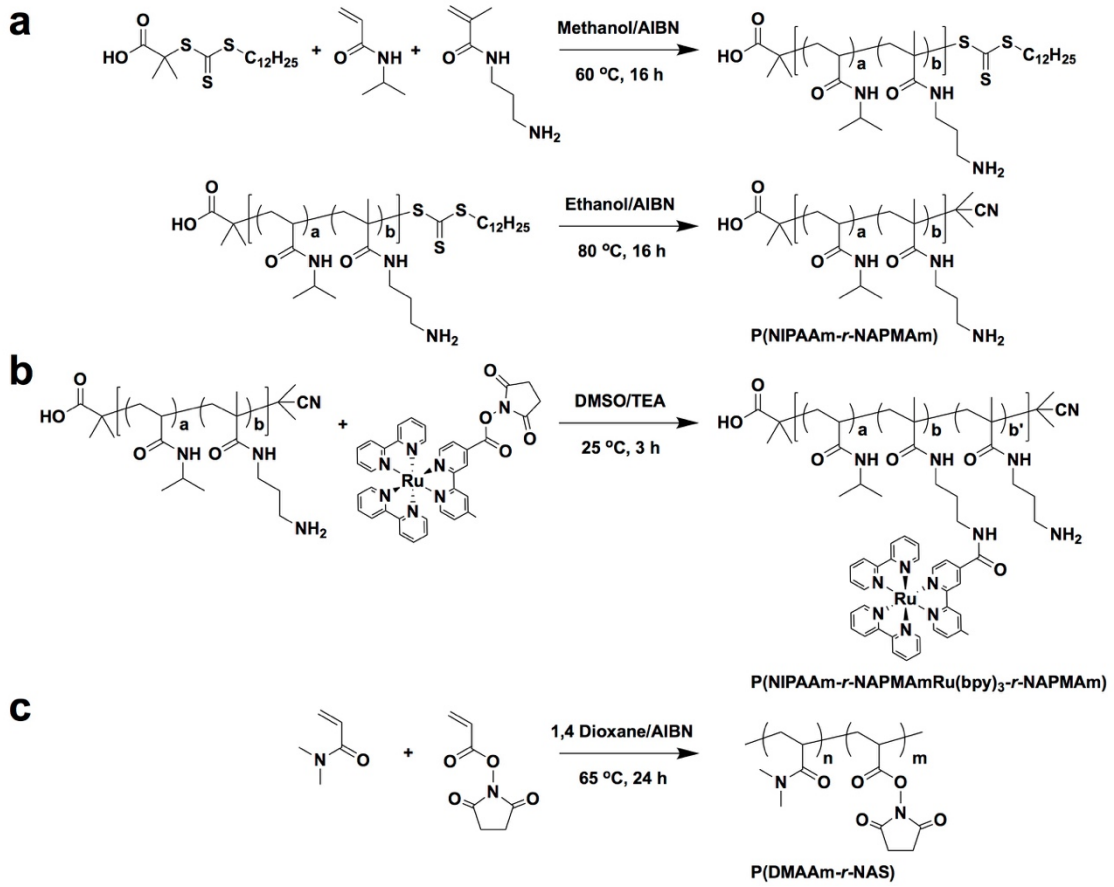

Figure 2-3. Synthetic procedure for copolymers. (a) the RAFT copolymerization of the P(NIPAAm-*r*-NAPMAm) copolymer, (b) the introduction of $Ru(bpy)_3$ group into the P(NIPAAm-*r*-NAPMAm) copolymer and (c) the random polymerization of P(DMAAm-*r*-NAS) as a cross linker, respectively

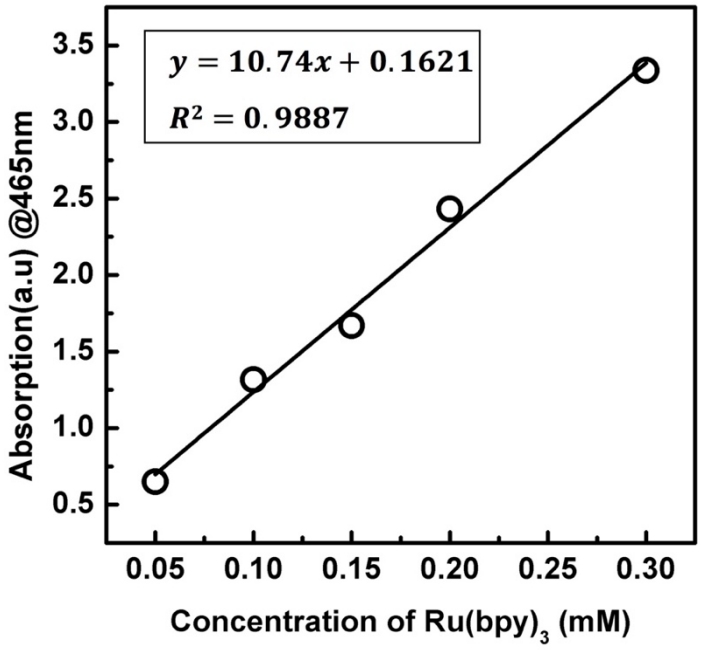

Figure 2-4. Calibration curve to calculate the amount of $Ru(bpy)_3$ conjugated to the copolymer chain. The curve was independently made from aqueous solutions of $Ru(bpy)_3Cl_2$ with known concentrations.

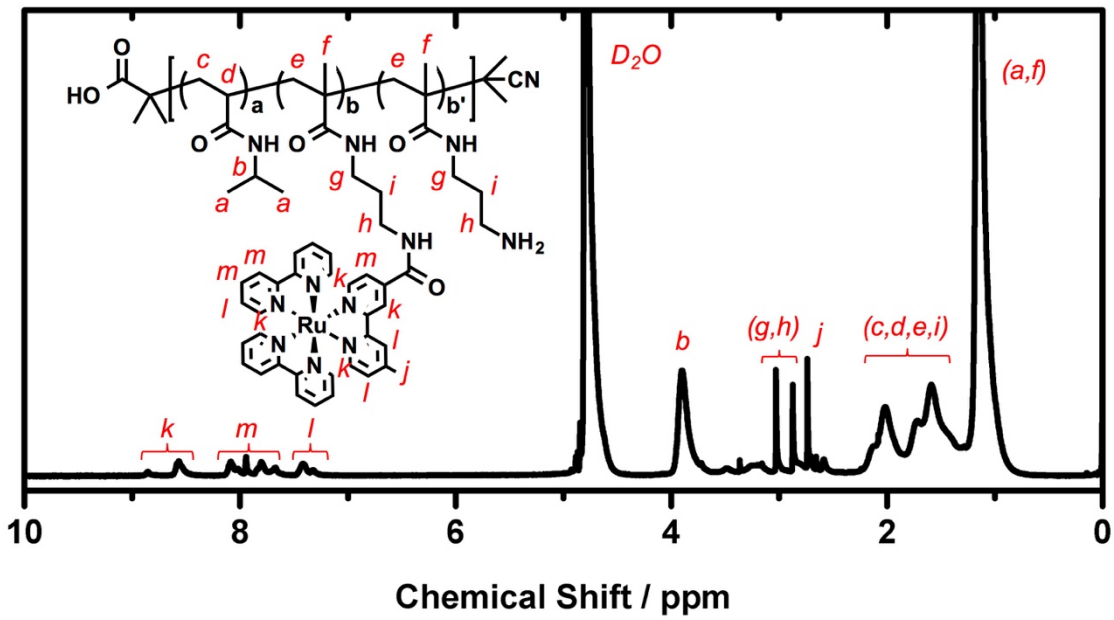

Figure 2-5. ^{1}H NMR spectrum of P(NIPAAm-*r*-NAPMAmRu(bpy)$_3$-*r*-NAPMAm).

2-2-4. Surface modification of magnetic nanoparticles by silanization and chemical conjugation

2-2-4-1. Preparation of amine functionalized magnetic nanoparticles

The 2 g of magnetic nanoparticles (soft ferrite), which have the hydroxyl group, were suspended in the 100 mL of deionized water by ultra-sonication for 1 min. And then, the magnetic nanoparticle suspension was transferred to 500 mL of 3-neck flask, and the deionized water was added until 300 mL. And then, the 40 μL of acetic acid was added into magnetic nanoparticles suspension, the mixture was bubbled with Ar for 20 min under mechanical stirring. And then, the 10 mL of APTES was injected into the mixture by using a syringe, and the reaction was then carried out at 70 °C for 16 hours. After the reaction, the mixture was cooled down to room temperature, and the treated magnetic nanoparticles were centrifuged 3 times at 1000 rpm for 3 min with methanol and vacuum-dried at room temperature for 1 day.

2-2-4-2. Preparation of vinyl functionalized magnetic nanoparticles

The amine functionalized magnetic nanoparticles, which were prepared in previous section, were suspended in the 100 mL of deionized water by ultra-sonication for 1 min. And then, the magnetic nanoparticle suspension was transferred to 500 mL of 3-neck flask, and the deionized water was added until 260 mL. The 1.21 g of NAS (about 10 times of mol of introduced primary amine) was dissolved in 40 mL of deionized water and then added into the magnetic nanoparticles suspension, the mixture was bubbled with Ar for 20 min under mechanical stirring. And then, 1 mL of TEA was added into the mixture, and the reaction was then carried out at 70 °C for 16 hours. After the reaction, the mixture was cooled down to room temperature, and the treated magnetic nanoparticles

were centrifuged 3 times at 1000 rpm for 3 min with methanol and vacuum-dried at room temperature for 1 day.

2-2-5. Characterization of modified magnetic nanoparticles

The hydrodynamic diameter of each magnetic nanoparticle was determined by DLS measurement (ELSZ-2000, otsuka). The zeta-potential was measured by Zetasizer Nano S (Melaven Panalytical). Infrared spectra of the magnetic nanoparticles were recorded on FT-IR420/IRT-30 (JASCO) by pressing the magnetic nanoparticles into a KBr pellet. The surface graft density of amine functionalized magnetic nanoparticles was calculated by the weight comparison of dried state and burned state of magnetic nanoparticles. The amine functionalized magnetic nanoparticles were burned in 800 ºC oven for 3 hours. And then, the weight was measured after cooling process.

2-2-6. Preparation of self-oscillating hydrogel physically containing magnetic nanoparticles

The self-oscillating hydrogel physically containing magnetic nanoparticles was prepared by the following protocol. First, the 60 mg of P(NIPAAm-*r*-NAPMAmRu(bpy)$_3$-*r*-NAPMAm) copolymer and 25 mg of magnetic nanoparticles (hard ferrite type) were dissolved in 0.5 mL of a tetraborate buffer solution, pH 9, in a vial. The 60 mg of P(DMAAm-*r*-NAS) g of a tetraborate buffer solution, pH 9, in another vial. Then, two solutions were mixed. The solutions with magnetic nanoparticles were prepared by a hand shake. After gelation, the prepared hydrogel was washed with deionized water to remove unreacted components for 2 days.

2-2-7. Preparation of self-oscillating hydrogel chemically containing magnetic nanoparticles depending on functional groups

2-2-7-1. The blending method with amine functionalized magnetic nanoparticles

The self-oscillating hydrogel containing chemically magnetic nanoparticles was prepared by the blinding method as following protocol. First, 50 mg of amine functionalized magnetic nanoparticles were suspended in 1 mL of a tetraborate buffer solution, pH 9, using the ultrasonication for 1 min, and then it was cooled down at 4 °C of the refrigerator for 1 hour. The 60 mg of P(NIPAAm-*r*-NAPMAmRu(bpy)$_3$-*r*-NAPMAm) copolymer was dissolved in 0.5 mL of magnetic nanoparticles suspension. The 60 mg of P(DMAAm-*r*-NAS) g of a tetraborate buffer solution, pH 9, in another vial. Then, two solutions were mixed and the concentration of magnetic nanoparticles in the final mixture was 25 mg/ml. After gelation, the prepared hydrogel was washed with deionized water to remove unreacted components for 2 days.

2-2-7-2. The grafting-onto method with vinyl functionalized magnetic nanoparticles

The self-oscillating hydrogel containing chemically magnetic nanoparticles was prepared by the following protocol. First, the 100 mg of vinyl functionalized magnetic nanoparticles were suspended in 5 mL of deionized water using an ultra-sonication, and then it was cooled down at 4 °C of the refrigerator for 1 hour. NIPAAm (509 mg, 9 mmol), NAPMAAm (89 mg, 1 mmol), and APS (54 mg, 0.25) were dissolved in the prepared magnetic nanoparticles suspension, and the pre-gel solution was degassed by dry Ar gas. And then, the gelation was started by injection of TEMED (20 μL). The prepared hydrogel was washed with deionized water for 2 days.

2-3. Results and discussions

2-3-1. Self-oscillating hydrogel physically containing magnetic nanoparticles

As a new approach for fabrication of self-oscillating hydrogels, the two types of linear copolymers with different functional groups was synthesized. One copolymer is a well-defined and self-oscillating material possessing $Ru(bpy)_3$ and primary amine groups. The detail-information of each segment could be calculated by ^{1}H-NMR and UV-vis spectrum, as shown in **Table 2-2**. Therefore, the Ru contents within hydrogel phase could be expected. The other copolymer is used for cross-linking, which is composed of hydrophilic DMAAm and NAS. Since NAS can react with primary amine groups forming amide bonds, the two copolymers can be readily cross-linked to afford a hydrogel. The first copolymers P(NIPAAm-*r*-NAPMAm) were synthesized *via* RAFT random copolymerization. $Ru(bpy)_3$, which is the catalyst for the BZ reaction, was post-modified into P(NIPAAm-*r*-NAPMAm) copolymers by a coupling reaction between the primary amine groups of NAPMAm and the NHS-$Ru(bpy)_3$, affording P(NIPAAm-*r*-NAPMAm$Ru(bpy)_3$-*r*-NAPMAm). P(DMAAm-*r*-NAS) was synthesized *via* free radical polymerization and was used for cross-linking.

Table 2-2. The results of P(NIPAAm-*r*-NAPMAm$Ru(bpy)_3$-*r*-NAPMAm) characterization**.** $Mn_{,}$ represent the number-averaged molecular weights of each segment before $Ru(bpy)_3$ coupling reaction. Ratio indicates the [NIPAAm]:[NAPMAm]. $N_{Ru(bpy)3}$ represent the average introduction number into the copolymer, respectively.

P(NIPAAm-*r*-NAPMAAmRu(bpy)$_3$-*r*-NAPMAm)				
$Mn_{,PNIPAAm}$ [a)]	$Mn_{,,PNAPMAm}$ [a)]	Ratio $_{mol\%}$ [a)]	PDI [b)]	$N_{Ru(bpy)3}$ [c)]
14.2 kDa	1.7 kDa	93:7	1.45	2.8

a) Calculated from ^{1}H NMR, b) Measured by GPC, c) Calculated from UV/Vis spectroscopy

This new approach based on the post cross-linking between P(DMAAm-*r*-NAS) and P(NIPAAm-*r*-NAPMAmRu(bpy)$_3$-*r*-NAPMAm) and could fabricate not only self-oscillating hydrogel but also the self-oscillating hydrogel physically containing magnetic nanoparticles. Typically, bare magnetic nanoparticles without additional treatments like surface modification by hydrophilic functional groups[18] rapidly precipitated in aqueous media. If such bare magnetic nanoparticles were directly introduced into the gel through a typical gelation reaction like free radical polymerization using a low molecular weight cross-linker, which requires at least several minutes for gelation, it would produce a heterogeneous hydrogel where most of the magnetic nanoparticles are localized at a bottom of the hydrogel. However, the coupling reaction kinetics between NAS and the primary amine groups can be controlled through the pH of the reaction solution, i.e., a higher pH value accelerates the coupling reaction kinetics [19]. In this cases, the pH of the pre-gel solution was adjusted to pH 9 to cause rapid gelation. Therefore, in this post cross-linking method between the two copolymers, gelation can be completed before precipitation of magnetic nanoparticles, typically within 10 seconds.

Based on these, the self-oscillating hydrogel physically containing magnetic nanoparticles was prepared by post cross-linking between P(NIPAAm-*r*-NAPMAmRu(bpy)$_3$-*r*-NAPMAm) and P(DMAAm-*r*-NAS) in an aqueous dispersion of magnetic nanoparticles, as shown in **Figure 2-6**. The magnetic nanoparticles were physically embedded within hydrogel networks without the sedimentation due to the rapid gelation and the absence of functional groups that can bind with hydrogel networks.

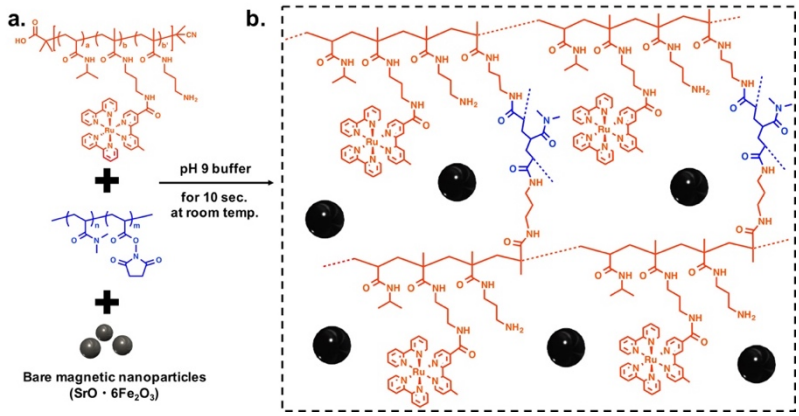

Figure 2-6. The schematic representation for preparation of self-oscillating hydrogel physically containing magnetic nanoparticles by using two types of copolymers and bare magnetic nanoparticles with the hydroxyl group. **(a)** Prepared copolymers and magnetic nanoparticles and **(b)** the chemical structure of the self-oscillating hydrogel physically containing magnetic nanoparticles.

2-3-2. Surface modification of magnetic nanoparticles by silanization and chemical conjugation

The general magnetic nanoparticles have the hydroxyl group or the hydrophobic functional groups depending on synthesis methods; therefore, the surface modification of magnetic nanoparticles has been carried out to disperse in aqueous media or to change to the functional surface. The silanization, which is a representative process of the surface modification, is the formation Fe-O-Si bond between nanoparticles and silane ligand; thus, the surface property can be modified by the terminal group of the silane agent[20].

In this study, the surface modification of magnetic nanoparticles was carried out by the silianization and the chemical conjugation, as shown in **Figure 2-7**. Bare magnetic nanoparticles with the hydroxyl group were silanized by APTES having primary amine terminal groups, and then the amine groups were modified to acryloyl groups having vinyl groups, by the chemical conjugation between amine and acryloyl-NHS groups.

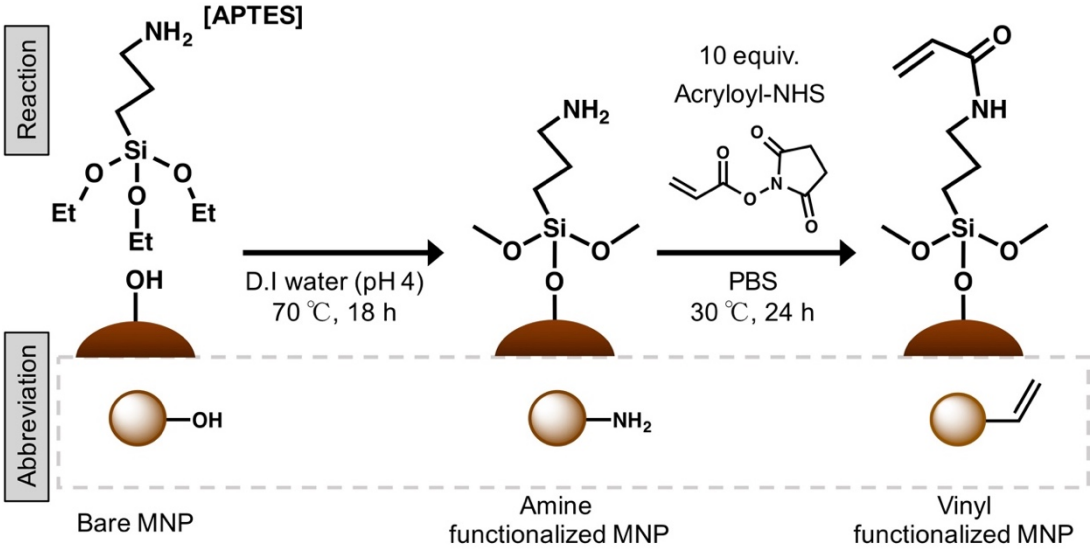

Figure 2-7. The schematic representation for the surface modification of magnetic nanoparticles, from hydroxyl to vinyl groups.

In order to confirm the terminal groups of each sample of magnetic nanoparticle, the FT-IR spectra were measured (**Figure 2-8**). The characteristic peak of the Fe-O bond was observed by the strong absorption band between 630 and 580 cm^{-1}, and the O-H stretching band was observed by the broad absorption band between 3600 and 3200 cm^{-1}; thus, it is shown that the bare magnetic nanoparticles have hydroxyl groups.

The bare magnetic nanoparticles were modified by APTES silane agents having terminal group of primary amine groups. Therefore, FT-IR spectrum of amine functionalized magnetic nanoparticles shown the characteristic peaks, such as the Si-O stretching and Si-O-H bending vibration between 960 and 870 cm^{-1}, and the Si-O-Si stretching band between 1150 to 1100 cm^{-1}, respectively. Besides, the broad stretching band of primary amine group was observed at 3450 cm^{-1}.

The vinyl functionalized magnetic nanoparticles were modified by the chemical conjugation between the primary amine and acryloyl-NHS groups: the functionalized

groups included the secondary amide bond. Therefore, the C=O stretching band of amide bonds was observed at 1650 cm^{-1}, and the N-H band of amide bond was observed at 3450 cm^{-1}, respectively.

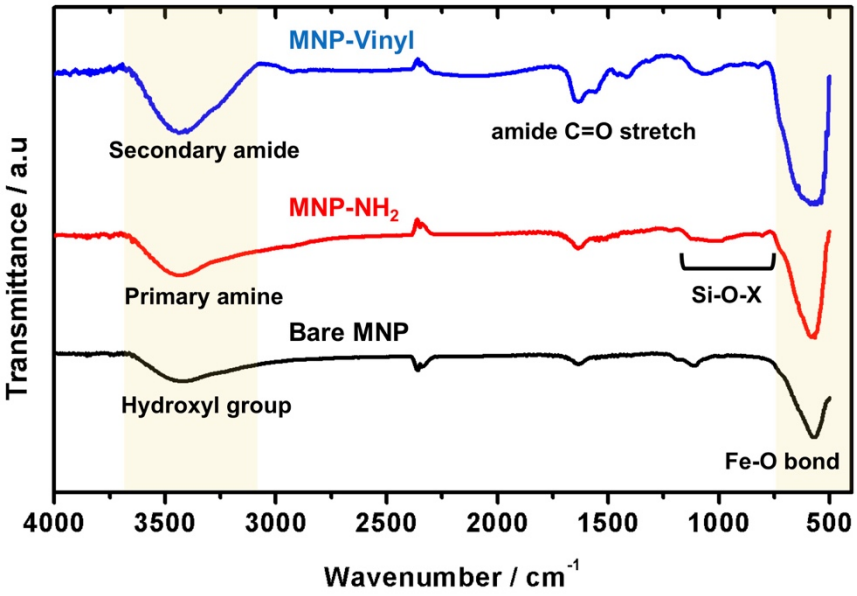

Figure 2-8. FT-IR spectra of magnetic nanoparticles depending on the surface functional groups. The black spectrum represents the bare magnetic nanoparticles with the hydroxyl group; the red spectrum represents amine functionalized magnetic nanoparticles; and the blue spectrum represents vinyl functionalized magnetic nanoparticles, respectively.

In addition, the hydrodynamic diameter and zeta-potential of magnetic nanoparticles ware measured, as shown in **Figure 2-9**. The hydrodynamic diameter of magnetic nanoparticles was measured in a low suspension concentration of about 10 mg/L, to prevent the interaction between nanoparticles[21]. The hydrodynamic diameter of bare magnetic nanoparticles was estimated to be 1 μm due to the hydrogen bonding between each nanoparticle having hydroxyl groups, despite having an average particles size of 100 nm. After silanization, however, the hydrodynamic size was decreased to about 220 nm

because the surface of each particles was modified by amine groups which can provide repulsive force between each nanoparticle. Finally, the hydrodynamic diameter of the vinyl functionalized magnetic nanoparticles was increased from 220 nm to 550 nm instead of maintaining, due to hydrogen bonding between oxygen and nitrogen of amide bonds. In addition, the zeta potential of magnetic nanoparticles was changed depending on the terminal groups. The zeta-potentials were measured as - 8 mV, 28 mV, and - 18 mV, as following the order of functional groups: hydroxyl, amine, and vinyl groups, respectively. Based on these results, it could be confirmed that the surface of magnetic nanoparticles was modified to surfaces having desired functional groups through the silanization and the chemical conjugation.

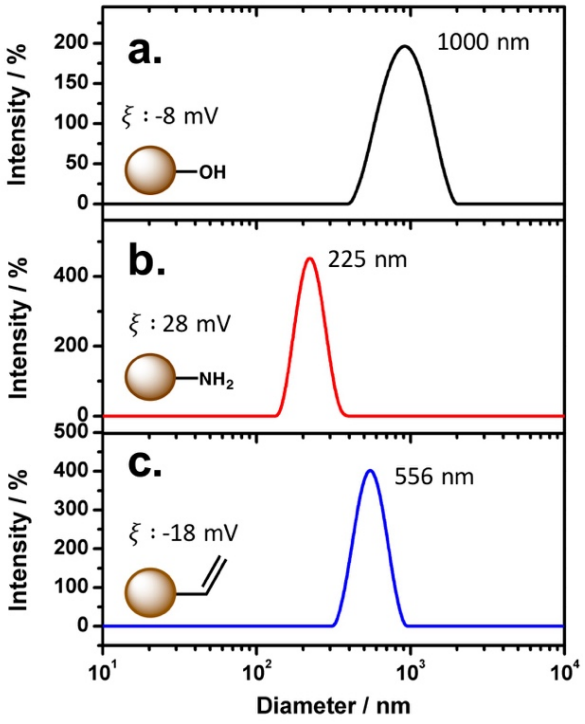

Figure 2-9. The hydrodynamic diameter and zeta-potential of magnetic nanoparticles. **(a)** bare, **(b)** amine functionalized, and **(c)** vinyl functionalized magnetic nanoparticles, respectively.

The surface graft density of amine functionalized magnetic nanoparticles was approximately calculated by the weight comparison of dried state and burned state of magnetic nanoparticles at 800 °C. During the heating process until 800 °C, the magnetic nanoparticles and silica layer can stand without a weight loss, while the terminal groups burned out; therefore, the weight loss occurs. In this study, the weight loss was estimated to be average 2.1 %; it means that the terminal groups/magnetic nanoparticles are 0.21 mg/g. However, the weight loss does not accurately provide the graft density of aminopropyl groups due to the non-uniform silica layer involving highly branched polycondensed structure[20]. In this study, however, the weight loss was converted to the graft density by molecular weight of the aminopropyl group ($NH_2C_3H_6$, 58.1 g/mol), to approximately estimate a minimum concentration of magnetic nanoparticles suspension required for the gelation. The graft density of aminopropyl groups onto the surface of magnetic nanoparticles was 0.36 mmol/g, approximately.

2-3-3. Self-oscillating hydrogel chemically containing magnetic nanoparticles

2-3-3-1. Post cross-linking with amine functionalized magnetic nanoparticles

The post cross-linking between P(NIPAAm-*r*-NAPMAmRu(bpy)$_3$-*r*-NAPMAm) and P(DMAAm-*r*-NAS) could also provide the preparation method of the self-oscillating hydrogel chemically containing magnetic nanoparticles, as shown in **Figure 2-10**. The amine functionalized magnetic nanoparticles participated in the formation of hydrogel networks by the chemical conjugation between P(DMAAm-*r*-NAS) chains. This chemical arrangement of magnetic nanoparticles was guaranteed by the reaction result between amine functionalized magnetic nanoparticles and P(DMMAm-r-NAS) copolymers excluding the P(NIPAAm-*r*-NAPMAmRu(bpy)$_3$-*r*-NAPMAm) copolymers. When mixed with P(DMMAm-r-NAS) copolymers, the amine functionalized magnetic

nanoparticles were changed to the encapsulated particles with micro-size due to the chemical conjugation between the amine and NAS groups. Therefore, they precipitated due to the absence of the P(NIPAAm-*r*-NAPMAmRu(bpy)$_3$-*r*-NAPMAm) copolymers, which can provide the main networks of the hydrogel.

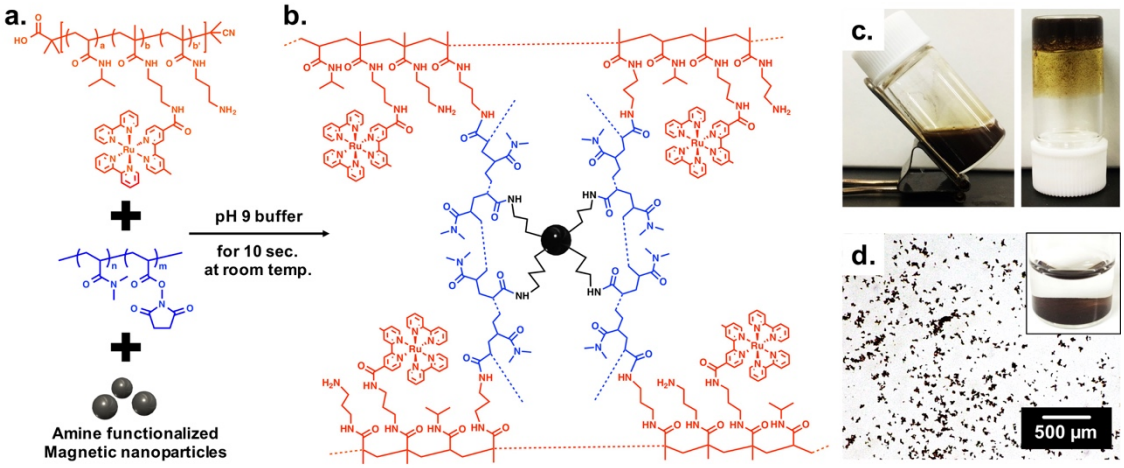

Figure 2-10. The schematic representation for preparation of self-oscillating hydrogel chemically containing magnetic nanoparticles by two types of copolymers and amine functionalized magnetic nanoparticles, and their images. **(a)** Prepared copolymers and amine functionalized magnetic nanoparticles, **(b)** the chemical structure of the self-oscillating hydrogel chemically containing magnetic nanoparticles, respectively. **(c)** The real images of pre-gel solution (left) and prepared hydrogel (right). **(d)** The microscopic and macroscopic (inset) images of polymer encapsulated magnetic particles with micro-size, which are prepared by the chemical conjugation between amine functionalized magnetic nanoparticles and P(DMAAm-*r*-NAS) random copolymers, respectively.

2-3-3-2. Grafting-onto method with vinyl functionalized magnetic nanoparticles

By using the grafting-onto method with vinyl functionalized magnetic nanoparticles, the self-oscillating hydrogel chemically containing magnetic nanoparticles

was also achieved, as shown in **Figure 2-11**. When polymerized in the pre-gel solution, the vinyl functionalized magnetic nanoparticles acted the cross-linker; therefore, the hydrogel could be prepared without low-molecular cross-linkers. And then, the self-oscillating hydrogel was achieved by the post-conjugation of $Ru(bpy)_3$-NHS. However, self-oscillating hydrogels prepared by the grafting-onto method have a concentration limitation of the vinyl functionalized magnetic nanoparticles. The dynamic behavior of self-oscillating hydrogel is due to the autonomous swelling/deswelling of the hydrogel networks by the BZ reaction[22-23]. However, if the concentration of vinyl functionalized magnetic nanoparticles is increased, the hydrogel networks can be composed of magnetic nanoparticles chains rather than polymer chains. Therefore, the increased magnetic nanoparticles can disturb the autonomous swelling/deswelling of hydrogel networks[24-25], despite the ongoing BZ reaction.

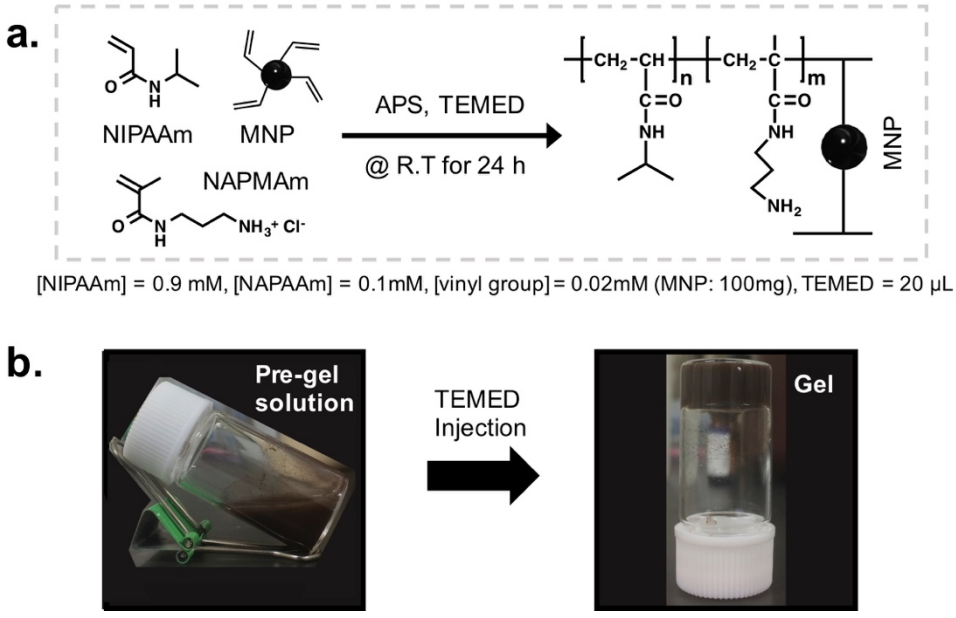

Figure 2-11. **(a)** Schemes for the self-oscillating hydrogel chemically containing magnetic nanoparticles by grafting-onto method. **(b)** The real images of pre-gel solution (left) and prepared hydrogel (right), respectively.

2-4. Conclusion

In this chapter, the self-oscillating hydrogels containing magnetic nanoparticles were prepared by following two methods: (1) the post cross-linking between P(NIPAAm-*r*-NAPMAmRu(bpy)$_3$-*r*-NAPMAm) and P(DMAAm-*r*-NAS) in an aqueous dispersion of magnetic nanoparticles and (2) the grafting-onto method with vinyl functionalized magnetic nanoparticles and monomers. Besides, they could be classified by the binding types between the hydrogel networks and magnetic nanoparticles, which determined by surface functional groups of magnetic nanoparticles.

Therefore, P(NIPAAm-*r*-NAPMAmRu(bpy)$_3$-*r*-NAPMAm) and P(DMAAm-*r*-NAS) copolymers were synthesized *via* RAFT and free radical random copolymerization, respectively. In addition, the bare magnetic nanoparticles with hydroxyl groups was modified to amine functionalized magnetic nanoparticles by the silane agent having amine terminal groups, and the amine functionalized magnetic nanoparticles were modified to vinyl functionalized magnetic nanoparticles by the chemical conjugation with acryloyl-NHS. Each surface functional group of magnetic nanoparticles was confirmed by FT-IR, DLS, and zeta-potential, respectively.

Based on these, the author introduced preparation methods of three types self-oscillating hydrogel containing magnetic nanoparticles, which distinguished by the physically embedded or the chemically bonded magnetic nanoparticles. Each self-oscillating hydrogels containing magnetic nanoparticles will be applied from the next chapters depending on research objects.

2-5. References

[1] C. R. Mayer, V. Cabuil, T. Lalot, R. Thouvenot, *Adv. Mater.* **2000**, *12*, 417.

[2] B. Séverine, L. Michael, W. Claire, L. Didier, G. Florence, M. Christine, L. V. Catherine, *Adv. Mater.* **2011**, *23*, 787.

[3] J. I. Kim, C. Chun, B. Kim, J. M. Hong, J.-K. Cho, S. H. Lee, S.-C. Song, *Biomaterials* **2012**, *33*, 218.

[4] R. Barbucci, D. Pasqui, G. Giani, M. De Cagna, M. Fini, R. Giardino, A. Atrei, *Soft Matter* **2011**, *7*, 5558.

[5] F. Roland, A. E. Kimon, L. N. Albert, S. W. Jan, *Small* **2009**, *5*, 383.

[6] Y. Li, G. Huang, X. Zhang, B. Li, Y. Chen, T. Lu, T. J. Lu, F. Xu, *Adv. Funct. Mater.* **2013**, *23*, 660.

[7] M. Zrinyl, H. G. Kilian, K. Dierksen, F. Horkay, *Macromol. Symp.* **1991**, *45*, 205.

[8] W. Haas, M. Zrinyi, H.-G. Kilian, B. Heise, *Colloid. Polym. Sci.* **1993**, *271*, 1024.

[9] Y. Wang, B. Li, Y. Zhou, D. Jia, *Nanoscale Research Letters* **2009**, *4*, 1041.

[10] N. A. D. Burke, H. D. H. Stöver, F. P. Dawson, *Chem. Mater.* **2002**, *14*, 4752.

[11] T.-Y. Liu, T.-Y. Chan, K.-S. Wang, H.-M. Tsou, *RSC Advances* **2015**, *5*, 90098.

[12] T. Mitsumata, A. Honda, H. Kanazawa, M. Kawai, *J. Phys. Chem. B* **2012**, *116*, 12341.

[13] R. Messing, N. Frickel, L. Belkoura, R. Strey, H. Rahn, S. Odenbach, A. M. Schmidt, *Macromolecules* **2011**, *44*, 2990.

[14] R. Weeber, S. Kantorovich, C. Holm, *Soft Matter* **2012**, *8*, 9923.

[15] B. M. Peek, G. T. Ross, S. W. Edwards, G. J. Meyer, T. J. Meyer, B. W. Erickson, *Int. J. Pept. Protein Res.* **1991**, *38*, 114.

[16] R. Tamate, T. Ueki, R. Yoshida, *Adv. Mater.* **2015**, *27*, 837.

[17] R. Tamate, T. Ueki, R. Yoshida, *Angew. Chem. Int. Ed.* **2016**, *55*, 5179.

[18] A. Dong, X. Ye, J. Chen, Y. Kang, T. Gordon, J. M. Kikkawa, C. B. Murray, *J. Am. Chem. Soc.* **2010**, *133*, 998.

[19] Y. Nojima, K. Iguchi, Y. Suzuki, A. Sato, *Biol. Pharm. Bull.* **2009**, *32*, 523.

[20] Y. Liu, Y. Li, X.-M. Li, T. He, *Langmuir* **2013**, *29*, 15275.

[21] J. Lim, S. P. Yeap, H. X. Che, S. C. Low, *Nanoscale research letters* **2013**, *8*, 381.

[22] R. Yoshida, T. Takahashi, T. Yamaguchi, H. Ichijo, *J. Am. Chem. Soc.* **1996**, *118*,

5134.

[23] R. Yoshida, E. Kokufuta, T. Yamaguchi, *Chaos: An Interdisciplinary Journal of Nonlinear Science* **1999**, *9*, 260.

[24] S. G. Starodubtsev, E. V. Saenko, M. E. Dokukin, V. L. Aksenov, V. V. Klechkovskaya, I. S. Zanaveskina, A. R. Khokhlov, *J. Phys.: Condens. Matter* **2005**, *17*, 1471.

[25] Y. Gao, S. C. F. Au-Yeung, C. Wu, *Macromolecules* **1999**, *32*, 3674.

Chapter 3:

Directional control of chemical wave propagation by magnetic migrations

3-1. Introduction

Traveling waves play an important role in mobility, mass transport, and signals in living systems, as shown in the peristaltic motion of organisms[1-2], cell migration through steady treadmilling of actin arrays[3], the auditory pathway of the cochlea[4], and the nervous system[5], *etc.* In particular, the peristaltic motion appearing in annelids[1] and digestive organs[2] involves a traveling wave, which generates a forward propulsive force for movement. Therefore, in the design of biomimetic/bioinspired functional materials, the implantation of a travelling wave is one of the essential factors to realize artificial locomotive materials. It is reported that the thermo-responsive hydrogel shows locomotion by sequentially applying localized heating along the hydrogel[6-8]. Moreover, a micro-robot made from a photo-responsive liquid crystal elastomer exhibits directional swimming upon a structural monochromatic light[9]. However, these motions depend on the application of external stimuli, and these materials are static in the absence of the external stimuli.

However, self-oscillating hydrogels shows not only an autonomous swelling/deswelling without the on-off switching of external stimuli[10-14] but also chemical wave propagation with peristaltic motion appears within the hydrogel. By using the chemical wave propagation and the following peristaltic motion, autonomous mass transport systems like an intestine have been reported[15-17]. However, it remains difficult to predict the exact direction of chemical wave propagation in the hydrogel because of its temperamentally and environmentally sensitive nature[18-19]. Therefore, it is a significant challenge to control the propagation direction of the chemical wave.

To date, research efforts into control over wave propagation in BZ reaction systems using hydrogels are mainly based on the geometrical regulation of hydrogels, as mentioned in Chapter 1.4. These methods can lead to the unidirectional propagation of

chemical waves within the hydrogel. However, they only cause a single direction of propagation during the BZ reaction because the propagation direction is determined at the start of the BZ reaction and is an inherent property of the system. Therefore, a feasible method for switching the propagation direction to a desired direction at a desired time within the hydrogel is still an unexplored area.

In this Chapter, the author introduced a new approach to control and switch the propagation direction of chemical waves through magnetic migration of the self-oscillating hydrogel physically containing magnetic nanoparticles in a liquid-liquid system composed of the aqueous BZ solution and an organic solvent such as hexane or dichloromethane (DCM). By magnetic migration of the self-oscillating hydrogel in the liquid layer system, the author could control not only the propagation direction but also the dynamic propagation behavior, such as a pause in the propagation and a switch in the propagation direction in an opposite way. This study may also provide a new concept for chemical systems in which the chemical environment regulates signal transmission.

3-2. Experiments section

3-2-1. Materials

N-isopropylacrylaminde (NIPAAm) was kindly provided by Kojin (Japan) and purified by recrystallization in toluene/n-hexane. *N*-(3-Aminopropyl) methacrylamide hydrochloride (NAPMAm) was purchased from Polyscience (USA) and used as received. Magnetic nanoparticles (Hard ferrite type, $SrO{\cdot}6Fe_2O_3$) was kindly provided Powdertech (Japan) and used as received. 2,2'-azobis (isobutyronitrile) (AIBN) was purchased from Wako Pure Chemical Industries (Japan) and was purified by recrystallization from methanol. Bis (2,2'-bipyridine) (1-(4'-methyl-2,2'-bipyridine-4- carbonyloxy)-2,5-pyrrolidinedione) ruthenium(II) bis(hexafluorophosphate) (abbreviated as $Ru(bpy)_3$-

NHS) was synthesized according to the previous report.[20] The chain transfer agent, S-1-dodecyl- S'-(*α*, *α*'-dimethyl- *α*''-acetic acid)-trithiocarbonate (DDMAT, purify >99 %), was purchased from Trylead Chemical Technology (China) and used as received. *N*-Acryloxysuccinimide (NAS) was purchased from Tokyo Kasei (Japan) and used as received. *N*, *N*-Dimethylacrylamide (DMAAm) was purchased from Wako Pure Chemical Industries (Japan) and used as received. All other chemicals were purchased from Wako Pure Chemical Industries (Japan) and used as received.

3-2-2. Preparation of self-oscillating hydrogel containing magnetic nanoparticles

The pre-gel solution was prepared in the same protocol in Section 2-2-6. Briefly, The P(NIPAAm-*r*-NAPMAmRu(bpy)$_3$-*r*-NAPMAm) copolymer and magnetic nanoparticles were dissolved in 0.5 mL of pH 9 buffer solution in a vial. The P(DMAAm-*r*-NAS) g of pH 9 buffer solution, in another vial. Then, two solutions were mixed. And then the mixture was quickly injected into a glass capillary with an inner diameter of 1.02 mm. After gelation through post cross-linking reaction, a glass capillary was moved to hot water bath (80°C) to separate a glass capillary and a shrunken hydrogel. The prepared hydrogel was washed with D. I water to remove unreacted components for 2 days.

3-2-3. SEM analysis of self-oscillating hydrogel containing magnetic nanoparticles

To analysis how magnetic nanoparticles were located in the hydrogel networks, the prepared self-oscillating hydrogel was characterized by using scanning electron microscopy (SEM). The self-oscillating hydrogels were lyophilized for 2 days and then carbon coated for observation. The images were obtained using a S4200 (Hitachi, Japan) operated at 10 kV accelerating voltage.

3-2-4. Observation of chemical wave propagation in the 2D hydrogel sheet

The self-oscillating hydrogel sheet was prepared in the same process as the cylindrical hydrogel using the space between two glass plates gapped with a silicone sheet (thickness 1 mm), instead of using a glass capillary. The hydrogel was cut to a size of 1 cm X 1 cm, and it was immersed in the solution containing the 894 mM of HNO_3 and 84 mM of $NaBrO_3$ for 20 min, to make the network more hydrophilic through the oxidation of $Ru(bpy)_3$ moieties. And then, the oxidized hydrogel was placed on the bottom of a dish containing low-density liquids. After that, the high-density liquid was carefully put on the hydrogel sheet by using a syringe. The aqueous BZ solution was consisted of 894 mM of HNO_3, 84 mM $NaBrO_3$ and 25 mM of Malonic acid (MA). The self-oscillating hydrogels were placed on the reaction media consisted of the BZ solution droplet/n-Hexane and the DCM droplet/BZ solution, respectively. And then, the chemical waves, which occurred in the localized area contacted the BZ solution, were monitored at 10 seconds intervals by using an optical microscope system (Keyence VH-5500, Japan). The time-course images were converted into gray level images by using the ImageJ (USA).

3-2-5. Observation of chemical wave propagation in the cylindrical hydrogel in liquid-liquid layers

The liquid-liquid layers were consisted of the aqueous BZ solution and water immiscible organic solvents such as hexane and dichloromethane (DCM). These solvents were accumulated in the glass cell (1.25 x 1.25 x 4.5 cm^3) by utilizing the difference of their density, in the following order: n-hexane/BZ solution/DCM. And then, the glass cell was placed onto a thermal plate that was set at 23 °C, and the room temperature was maintained at 19 °C. The prepared cylindrical hydrogel was cut to a length of about 10 mm, and it was immersed in the solution containing the 894 mM of HNO_3 and 84 mM of

$NaBrO_3$ for 20 min. The hydrogel was vertically placed in the glass cell containing the two or three liquid layers. Then, it was magnetically shifted depending on experimental conditions. Propagation behaviors of chemical waves were observed and the image processing was done in the same manner as before.

3-3. Results and discussions

3-3-1. Chemical wave propagation in 2D hydrogel sheet

First, the aspects of chemical wave propagation within 2D self-oscillating hydrogel sheets were investigated when they are in reaction environments composed of an aqueous BZ solution and organic solvents immiscible in water. The higher density liquid was placed on the surface of the hydrogel sheet as a droplet. The lower density liquid occupied extra space excluding the droplet. Thus, reaction environments consisted of (a) a DCM droplet/BZ solution and (b) a BZ solution droplet/hexane, as shown in **Figure 3-1**. Chemical waves occurred within a localized area in the hydrogel sheet that was in contact with the BZ solution, while the area contacting with organic solvents maintained a paused state due to the blocking of the reactant. The regularity in the propagation of chemical waves could be observed; they started in the BZ solution and propagated to the interface between the two liquids. This propagation behavior showed the possibility that the propagation direction of chemical waves could be controlled by the position of the liquid interface.

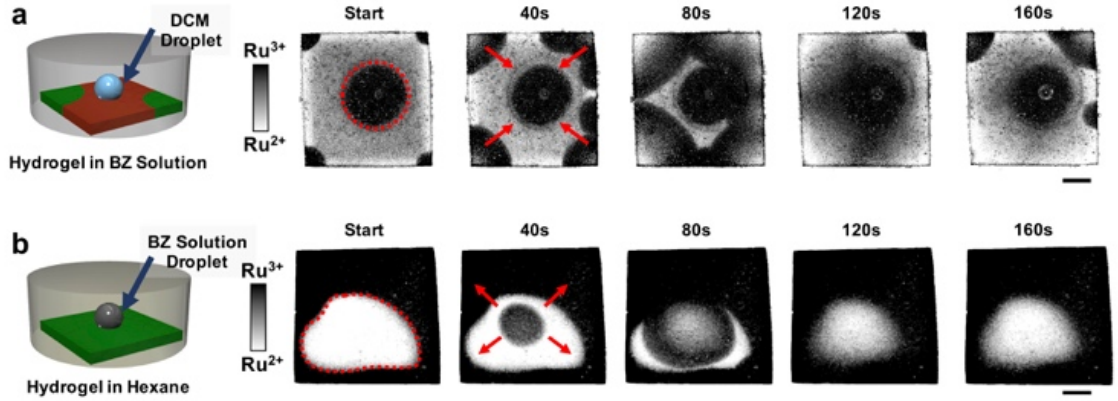

Figure 3-1. Time resolved images of chemical wave propagation within 2D self-oscillating hydrogel sheets in the aqueous BZ solution and organic solvents immiscible with water reaction medium. (a) DCM droplet/BZ solution and (b) BZ solution droplet/hexane, respectively. The red dashed circles indicate liquid interfaces, and the red arrows indicate propagation directions, respectively. (scale bar: 2 mm)

3-3-2. Preparation of self-oscillating hydrogel containing magnetic nanoparticles and design of the liquid layer system containing the liquid-liquid interface

However, it is still difficult to switch a propagation direction during the BZ reaction due to a fixed arrangement. If a position of a self-oscillating hydrogel can be freely modulated in a system composed of two interfaces, it can be expected to switch a propagation direction depending on the interface position in which the self-oscillating hydrogel fixed. Therefore, the author designed the magnetically sensitive self-oscillating hydrogel to freely modulate the position using a magnet, without any physical contact. This is because the physical contact for a position modulation can interfere with the BZ reaction.

The magnetic migration can be achieved by small contents of magnetic nanoparticles regardless of bonding types in the hydrogel network, therefore, the self-oscillating hydrogel physically containing magnetic nanoparticles was introduced and

prepared by the bare magnetic nanoparticles and post cross-linking between P(NIPAAm-*r*-NAPMAmRu(bpy)$_3$-*r*-NAPMAm) and P(DMAAm-*r*-NAS) copolymers, due to the physically embedded structure.

By taking advantage of the regularity in the propagation of chemical waves by the liquid interface, the liquids were accumulated in the glass cell by utilizing density differences in the following order: n-hexane/BZ solution/DCM; this arrangement provided two liquid interface. Therefore, the directional control of chemical waves propagation was attempted by magnetic migrations, and regularity in the propagation of chemical waves by liquid interfaces, as shown in **Figure 3-2**.

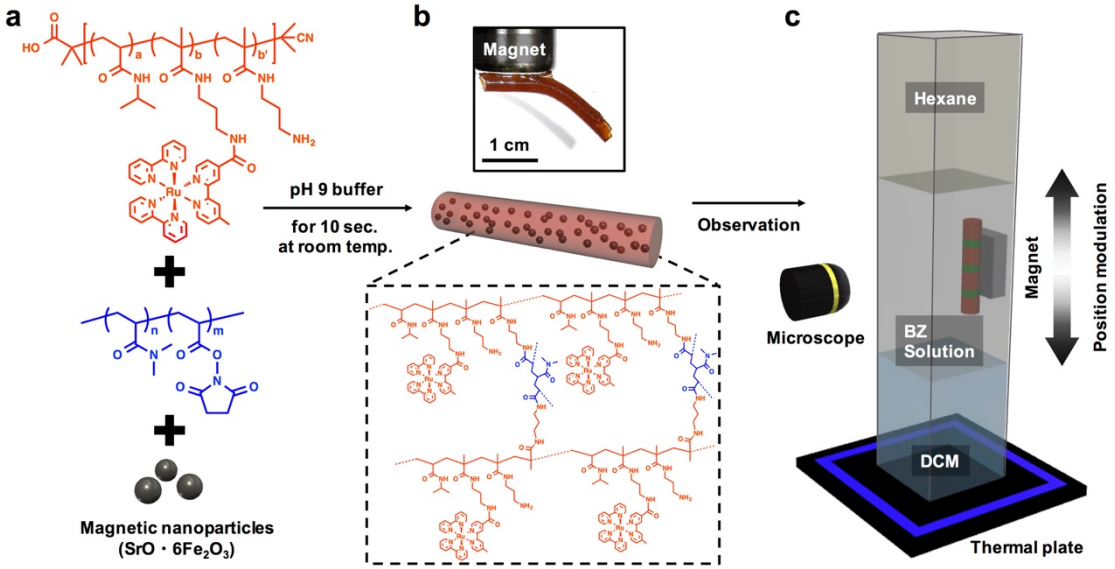

Figure 3-2. Schematic representation for the preparation of the self-oscillating hydrogel containing magnetic nanoparticles and observation of chemical wave propagation. **(a)** Prepared copolymers and magnetic nanoparticles, **(b)** the real image (upper) and chemical structure (lower) of the self-oscillating hydrogel containing magnetic nanoparticles, and **(c)** observation of chemical wave propagation by magnetic migration.

3-3-3. SEM analysis of self-oscillating hydrogel containing magnetic nanoparticles

After gelation, how magnetic nanoparticles are distributed in the hydrogel networks was investigated by using a scanning electron microscope (SEM) and a lyophilized hydrogel (**Figure 3-3**). If the magnetic nanoparticles were positioned so closely, applying a magnetic field could influence hydrogel networks to form an aligned structure along the direction of the magnetic field[21]. According to the reported equation (a) [22], the critical distance between magnetic nanoparticles required to cause such network transformation can be roughly calculated.

$$d = d_m(\emptyset^{-1/3} - 1) \qquad \text{(a)}$$

where d_m and $\emptyset$ represent the diameter and the volume fraction of magnetic nanoparticles. In this study, the volume fraction of the magnetic nanoparticles was 5.2 x 10^{-3}, the average diameter of the aggregated magnetic nanoparticles was about 12 μm. The calculated results show that the critical distance was about 50 μm. However, the SEM images showed that the distance between aggregated magnetic nanoparticles was around 60 μm, which is longer than the critical distance (**Figure 3-3**). Therefore, the prepared self-oscillating hydrogel could be attached to a magnet without causing deformation of the hydrogel networks, as shown in **Figure 3-2b**.

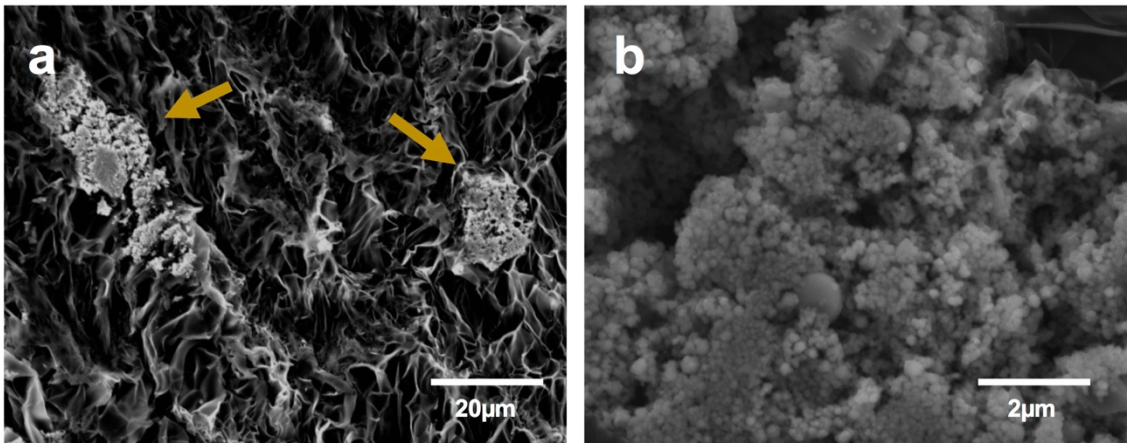

Figure 3-3. SEM images of a microstructure in the self-oscillating hydrogel containing magnetic nanoparticles. **(a)** The SEM image of the hydrogel networks and aggregated magnetic nanoparticles. **(b)** The SEM image of the aggregated magnetic nanoparticles indicated by the left arrow.

3-3-4. Chemical wave propagation in the cylindrical hydrogel in liquid-liquid layers

First, the cell container was filled with two liquid layers, where the BZ solution and hexane formed the lower and upper layers, respectively (**Figure 3-4a**). When the hydrogel was vertically fixed at the interface of the hexane/BZ solution by a neodymium magnet (500 mT), the BZ reaction occurred only in the partial body of the hydrogel immersed in the BZ solution (the left image). We note that the vertically placed hydrogel was observed in the front view, and thus there was a boundary of organic solvent/the BZ solution at the backside of the hydrogel owing to the meniscus (**Figure 3-5**). We indicate such boundaries using dashed lines in **Figure 3-4**. The limited region of the hydrogel immersed in the BZ solution only exhibited a chemical wave, which was generated by periodic autonomous redox change of $Ru(bpy)_3$ in the hydrogel during the BZ reaction. The produced chemical waves propagated at a constant speed along the axis of the hydrogel in an upward direction from the bottom to the boundary of the interface of

hexane/BZ solution. On the other hand, the residual part of the hydrogel immersed in hexane was constantly kept in an oxidized state and showed a green color. This was because our hydrogel was initially oxidized in the solution containing HNO_3 and $NaBrO_3$ before being dipped in the cell container. The oxidized state of the hydrogel was maintained in the organic solvents, keeping it isolated from the progressive BZ reaction.

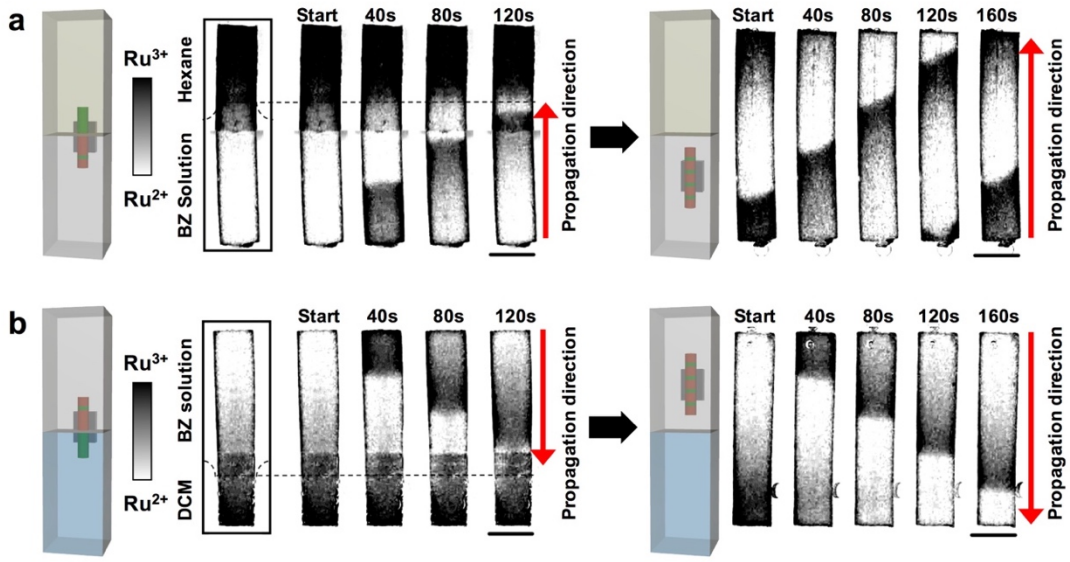

Figure 3-4. Time resolved images of chemical wave propagation when the hydrogel was fixed at the interface (left) and in the BZ solution after magnetic migration (right). The interfaces are **(a)** hexane/BZ solution and **(b)** BZ solution/DCM (scale bar: 2 mm).

The hydrogel was kept at the interface of the hexane/BZ solution for 1 hour, and then magnetically shifted to the lower phase of the BZ solution so that the entire hydrogel structure was immersed in the solution. Then, after several minutes, the chemical waves started to propagate from the bottom to the top edge of the hydrogel (upward propagation), as shown in the right panels in **Figure 3-4a**. This upward propagation was maintained for several hours until the BZ reaction finished.

On the other hand, when the hydrogel was vertically fixed at the interface of the BZ solution/DCM (left panels in **Figure 3-4b**), the produced chemical waves propagated at a constant speed along the long axis of the hydrogel in a downward direction from the top to the boundary of the interface of the BZ solution/DCM. After staying at the interface for 1 hour, the hydrogel was magnetically shifted to the upper phase of the BZ solution. Then, after several minutes, chemical waves propagated downward in the hydrogel from the top to the bottom edge (right panels in **Figure 3-4b**). Note that this direction was opposite from the case of the hexane/BZ solution, as shown in **Figure 3-4a**.

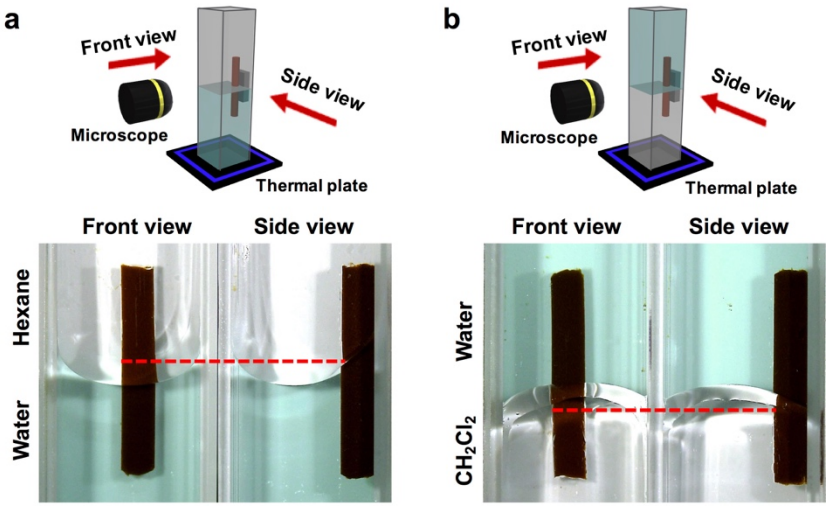

Figure 3-5. Apparent boundary of the water/water-immiscible organic solvent layer caused by the meniscus: **(a)** hexane/water and **(b)** water/DCM, respectively. The water was dyed with blue edible dye to distinguish the different layers. The dashed line denotes the real boundary.

The chemical wave patterns depend on the shape of the hydrogel. Typically, chemical waves tend to be initiated at the edges or corners and propagate to the center of the hydrogel since the probability to encounter the substrates for the BZ reaction is higher

at the edges and corners than at the center of the hydrogel. In the case of 1-dimensional shapes like the cylindrical gel, the hydrogel has two edges with the same probability to function as an initiating point for the chemical wave. Accordingly, chemical waves should be initiated from both edges of the hydrogel and propagate inwards intrinsically. After the two chemical waves generated at both edges, the surviving waves with higher frequency determine the direction of propagation within the hydrogel[18-19]. However, the oscillating behavior of the BZ reaction is well known to be fluctuation under minor changes in the experimental conditions. Thus, the chemical wave patterns are not stable and often change their propagation direction. For example, it was reported that the chemical wave patterns were different between the initial and later stages (after approximately 30 min) of the BZ reaction[18]. Therefore, it is difficult to predict the actual chemical wave propagation direction within the hydrogel because multiple pattern formation modes with several ignition points often emerge as time passes. In contrast, our cylindrical hydrogel showed a single mode of the propagation after the direction was determined to be either upward or downward. Subsequently, propagation continuously maintained its direction until the reaction finished.

3-3-5. Times required to reach unidirectional propagation depending on the fraction of hydrogel length immersed in the BZ solution

How the fraction of hydrogel length immersed in the BZ solution at the interface affects the time required to reach unidirectional chemical wave propagation of between the edges was investigated. The hydrogels were placed at the interface of the BZ solution/DCM with different immersion length fractions in each phase. When 51% of the hydrogel length was initially immersed in the BZ solution at the interface (the left image of **Figure 3-4a**), part of the hydrogel exhibited continuous downward chemical wave

propagation up to the boundary of the BZ solution/DCM. After 1 hour, the whole of the hydrogel was readily shifted to the BZ solution layer. Then the hydrogel started to reveal a collision between the pre-established downward waves and newly generated waves, as shown in the time resolved images in **Figure 3-6a**.

Temporal evolution of wave propagation was analyzed by image binarization of the green color signal intensity corresponding to the oxidized state in the hydrogel (lower images of **Figure 3-6a**). In the initial stage, the upper 51% of the hydrogel structure exhibited stable downward propagation of waves, whereas the residual lower part of the hydrogel stayed in a static oxidized state. After 15 minutes, new target waves were generated in the lower part of the hydrogel. When these newly generated waves encountered downward waves, the downward waves immediately disappeared. As a result, the chemical wave patterns in the entire hydrogel took on a different phase, where the waves propagate in both the upward and downward directions simultaneously. This behavior is shown in the two middle panels in **Figure 3-6a**. After more than 2 hours, unidirectional propagation in the downward direction became dominant and was maintained until the BZ reaction finished. These results indicate that the previously determined unidirectional propagation remains latent in the hydrogel. The intrinsic wave propagation direction reappears 2 hours later, although the unidirectional propagation once fades out as a consequence of the destructive interference during the BZ reaction.

In addition, the wave propagation behavior in another condition was investigated, where 72% of the hydrogel length and was initially immersed in the BZ solution at the interface (the left image of **Figure 3-6b**). After the entire hydrogel was shifted towards the BZ solution layer, there was a collision between the pre-established downward waves and newly generated upward waves, as shown in the images in **Figure 3-6b**. In this case, it took only 35 minutes to reach downward wave propagation in the hydrogel. This

downward propagation was maintained until the BZ reaction finished. These results indicate that the larger immersed area of the hydrogel in the BZ solution imparts more stability to the unidirectional propagation of chemical waves in the hydrogel, shortening the time required for reaching unidirectional propagation through the hydrogel.

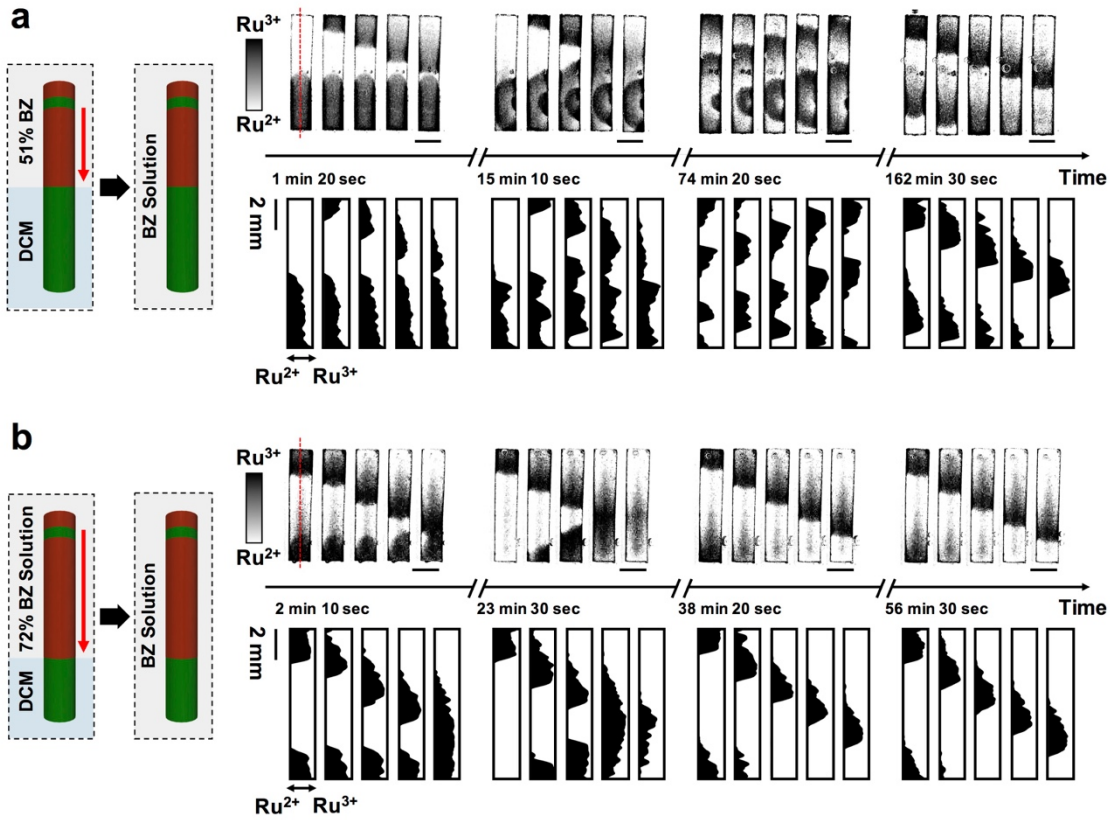

Figure 3-6. Difference in the times required to reach unidirectional propagation in the hydrogel depending on the fraction of hydrogel length immersed in the BZ solution. **(a)** 51 % and **(b)** 72 % of the hydrogel length was initially immersed in the BZ solution. Time resolved images represent propagation behaviors 30 second intervals at each step after shifting the hydrogels to the BZ solution. The lower set of time resolved images in each figure represents the binarized images of the waveforms analyzed from the gray level intensity of Ru^{3+} (scale bar: 2 mm).

3-3-6. Reversible propagation of chemical waves depending on hydrogel positions

By taking advantage of such an easy method to regulate the propagation direction of chemical waves and shorten the time required to reach unidirectional propagation, this system for reversibly switching the propagation direction of waves in a single hydrogel was further elaborated. No self-oscillating hydrogel has been reported to exhibit such reversible switching of propagation direction[15-19, 23-27]. First, three liquid layers composed of hexane, BZ solution, and DCM were prepared (**Figure 3-7**). The hydrogel was initially placed at the interface of the BZ solution/DCM (Step 1) and was then shifted to the BZ solution layer (Step 2). In accordance with our previous results, the hydrogel showed downward wave propagation (**Figure 3-8b**). After that, it was directly shifted and placed at the interface of the hexane/BZ solution. However, the hydrogel maintained downward propagation, even at the interface of the hexane/BZ solution, where the propagation direction is expected to be upward (**Figure 3-8a**). This is because fully grown waves with downward propagation were too stable to produce new upward propagation toward the interface of hexane/BZ solution.

Thus, the hydrogel, whose propagation direction was determined to be downward, was shifted to the hexane layer so as to be completely surrounded by the organic solvent (Pause 1). Then, chemical wave propagation stopped in the hydrogel and stayed in the oxidized state (**Figure 3-8b**). When the oxidized hydrogel in the hexane layer was shifted and placed at the hexane/BZ solution interface again (Step 3), upward wave propagation began (**Figure 3-8c**). After that, the hydrogel was placed in the BZ solution (Step 4) and upward waves propagated throughout the hydrogel. The hydrogel was sequentially shifted to the DCM layer through the BZ solution/DCM interface (Pause 2), and there the waves completely disappeared (**Figure 3-8c**). With the reverse shift of the hydrogel, downward wave propagation started when the hydrogel was at the interface (Step 5) same

as in Step 1. Further, the wave propagated thorough the whole hydrogel in the BZ solution (Step 6), same as in Step 2. Note that, by immersing the hydrogel in the organic solvent, the propagation of chemical waves in the hydrogel could be temporary paused and resumed at the desired time by shifting it to the organic solvent/BZ solution interfaces. Moreover, the propagation direction of the chemical wave reversibly switched between upward and downward directions by changing the position of the hydrogel.

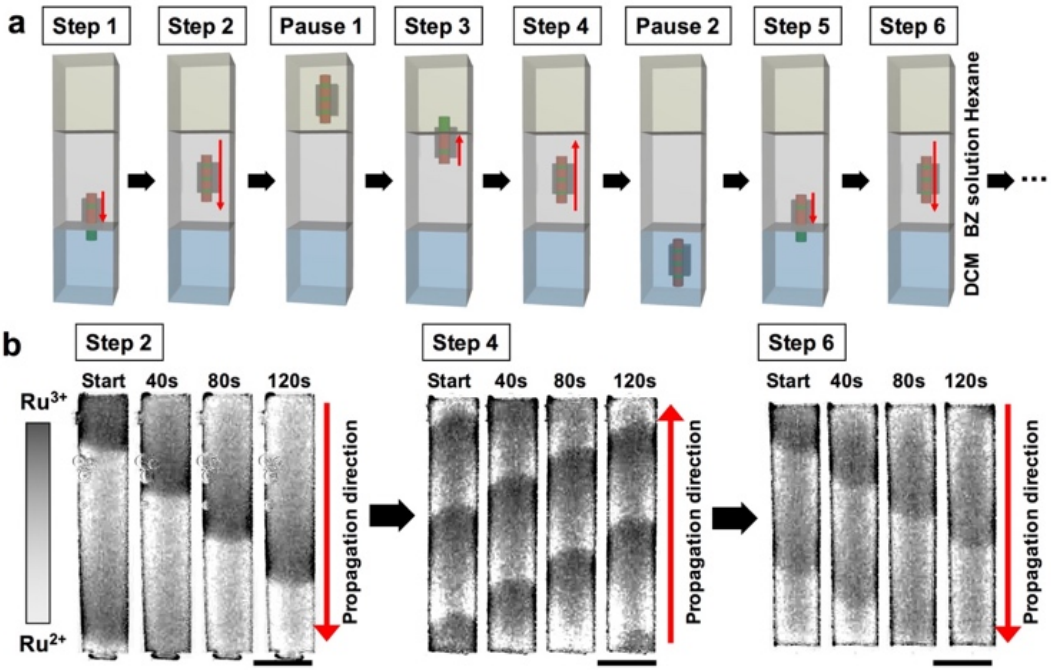

Figure 3-7. Reversible propagation of chemical waves depending on hydrogel position. **(a)** Schematic image of hydrogel position modulation by magnetic migration and **(b)** time resolved images of unidirectional chemical waves propagating reversibly in each step (scale bar: 2 mm).

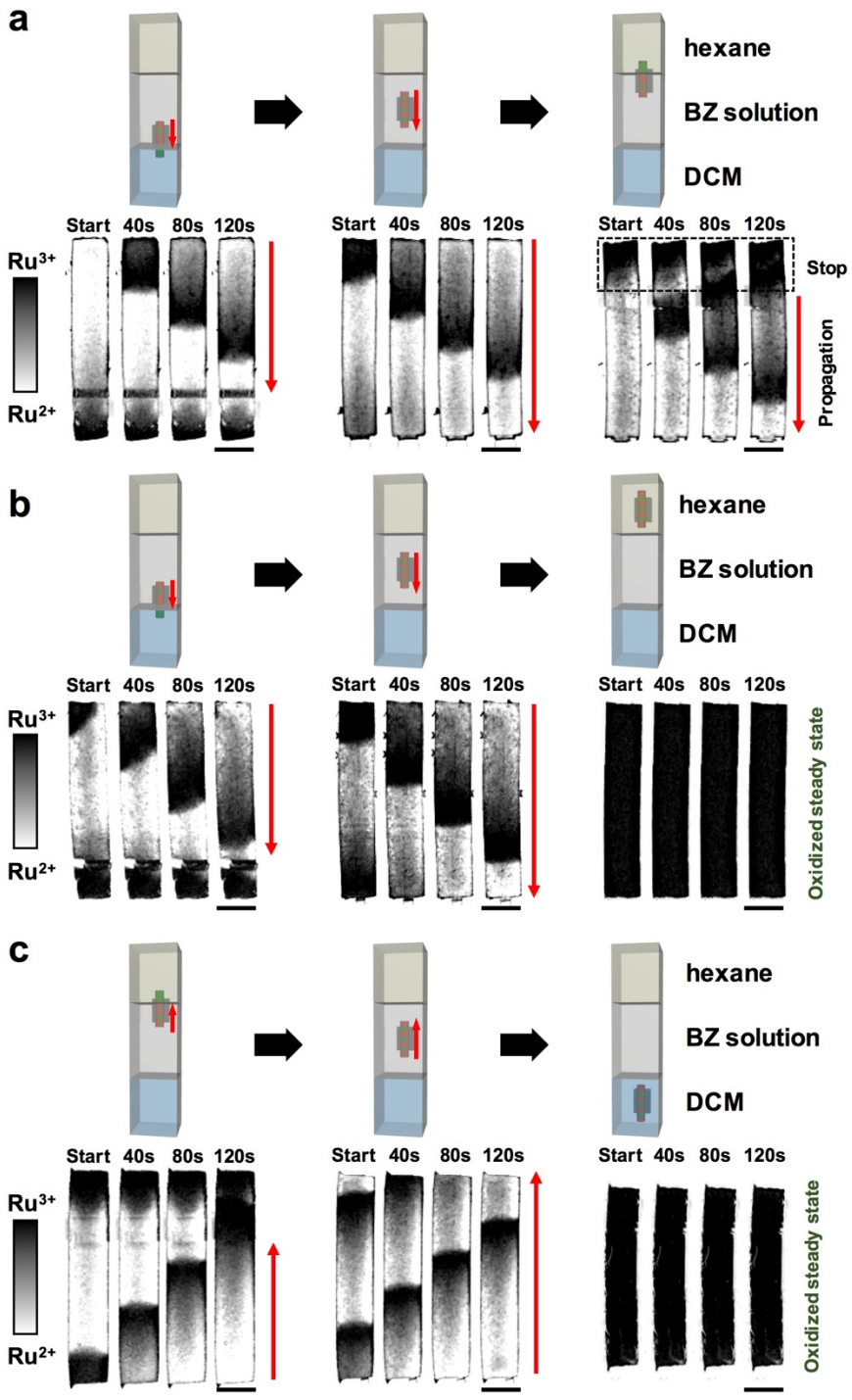

Figure 3-8. The propagation behaviors of chemical waves when hydrogel with the unidirectional wave was magnetically shifted to the following positions; **(a)** the opposite interface composed of hexane and BZ solution, **(b)** hexane layer and **(c)** DCM layer, respectively. (scale bar: 2 mm)

3-4. Conclusion

In this chapter, the author investigated how the propagation direction of a chemical wave could be controlled *via* magnetic migration of the self-oscillating hydrogel with a change in the position of liquid interface. The self-oscillating hydrogel physically containing magnetic nanoparticles was prepared by a rapidly occurring post cross-linking method. Due to magnetic nanoparticles embedded in the hydrogel network, the self-oscillating hydrogel could be magnetically fixed or shifted in liquid-liquid layers consisting of the aqueous BZ solution and water-immiscible organic solvents. When the hydrogel was magnetically fixed at the liquid interfaces, chemical wave propagation occurred only in the hydrogel portion immersed in the BZ solution. On the other hand, the residual portion of the hydrogel immersed in organic solvents maintained a paused state. In this state, the chemical waves propagated to the liquid interface at a constant speed starting from the edge of the hydrogel immersed in the BZ solution. Therefore, the propagation direction of chemical waves was determined by the relative position of the liquid interface with respect to the hydrogel. Moreover, a unidirectional chemical wave could propagate within the hydrogel when it was magnetically shifted to the BZ solution. The time required for reaching unidirectional propagation of chemical waves depended on the length fraction immersed in each phase. Unidirectional chemical wave propagation was imparted faster when a larger fraction of the hydrogel was immersed in the BZ solution.

Based on the results that the propagation direction was easily regulated and the time to reach unidirectional propagation was shortened, it was possible to reversibly switch the direction of the chemical wave in a targeted way at a desired time by manipulating the position in the liquid system. Finally, the author believe that this study contributes to the design of functional soft materials having autonomous mobility because

the chemical wave propagation direction can be controlled in an easy way, and reversible propagation at a desired time can be achieved.

3-5. References

[1] K. Quillin, *J. Exp. Biol.* **1998**, *201*, 1871.

[2] R. R. Seeley, T. Stephens, P. Tate, in *Anatomy & physiology. 6th* McGraw Hill, Boston, p. 860.

[3] J. Allard, A. Mogilner, *Curr. Opin. Cell Biol.* **2013**, *25*, 107.

[4] D. Purves, G. Augustine, D. Fitzpatrick, L. Katz, A. LaMantia, J. McNamara, S. Williams, in *Neuroscience 3rd Edition.* , Sinauer Associates, Inc., Sunderland (MA) **2004**, p. 289.

[5] Y. Yamaguchi, in *Advances in Cognitive Neurodynamics (iii): Proceedings of the Third International Conference on Cognitive Neurodynamics-2011*, Springer, **2013**, p. 213.

[6] L. Yeghiazarian, S. Mahajan, C. Montemagno, C. Cohen, U. Wiesner, *Adv. Mater.* **2005**, *17*, 1869.

[7] E. Wang, M. S. Desai, S.-W. Lee, *Nano Lett.* **2013**, *13*, 2826.

[8] A. W. Hauser, A. A. Evans, J. H. Na, R. C. Hayward, *Angew. Chem. Int. Ed.* **2015**, *54*, 5434.

[9] S. Palagi, A. G. Mark, S. Y. Reigh, K. Melde, T. Qiu, H. Zeng, C. Parmeggiani, D. Martella, A. Sanchez-Castillo, N. Kapernaum, *Nature Materials* **2016**, *15*, 647.

[10] R. Yoshida, T. Takahashi, T. Yamaguchi, H. Ichijo, *J. Am. Chem. Soc.* **1996**, *118*, 5134.

[11] R. Yoshida, T. Ueki, *NPG Asia Materials* **2014**, *6*, e107.

[12] R. Tamate, T. Ueki, R. Yoshida, *Adv. Mater.* **2015**, *27*, 837.

[13] R. Tamate, T. Ueki, R. Yoshida, *Angew. Chem. Int. Ed.* **2016**, *55*, 5179.

[14] Y. S. Kim, R. Tamate, A. M. Akimoto, R. Yoshida, *Mater. Horizons* **2017**, *4*, 38.

[15] S. Maeda, Y. Hara, R. Yoshida, S. Hashimoto, *Angew. Chem.* **2008**, *120*, 6792.

[16] Y. Murase, S. Maeda, S. Hashimoto, R. Yoshida, *Langmuir* **2008**, *25*, 483.

[17] Y. Shiraki, R. Yoshida, *Angew. Chem. Int. Ed.* **2012**, *51*, 6112.

[18] I. C. Chen, O. Kuksenok, V. V. Yashin, R. M. Moslin, A. C. Balazs, K. J. Van Vliet, *Soft Matter* **2011**, *7*, 3141.

[19] P. Yuan, O. Kuksenok, D. E. Gross, A. C. Balazs, J. S. Moore, R. G. Nuzzo, *Soft Matter* **2013**, *9*, 1231.

[20] B. M. Peek, G. T. Ross, S. W. Edwards, G. J. Meyer, T. J. Meyer, B. W. Erickson, *Int. J. Pept. Protein Res.* **1991**, *38*, 114.

[21] T.-Y. Liu, T.-Y. Chan, K.-S. Wang, H.-M. Tsou, *RSC Adv.* **2015**, *5*, 90098.

[22] T. Mitsumata, A. Honda, H. Kanazawa, M. Kawai, *J. Phys. Chem. B* **2012**, *116*, 12341.

[23] T. Masuda, A. M. Akimoto, K. Nagase, T. Okano, R. Yoshida, *Sci. adv.* **2016**, *2*, e1600902.

[24] S. Tateyama, Y. Shibuta, R. Yoshida, *J. Phys. Chem. B* **2008**, *112*, 1777.

[25] K. Homma, T. Masuda, A. M. Akimoto, K. Nagase, K. Itoga, T. Okano, R. Yoshida, *Small* **2017**, *13*.

[26] V. V. Yashin, S. Suzuki, R. Yoshida, A. C. Balazs, *J. Mater. Chem.* **2012**, *22*, 13625.

[27] X. Lu, L. Ren, Q. Gao, Y. Zhao, S. Wang, J. Yang, I. R. Epstein, *Chem. Commun.* **2013**, *49*, 7690.

Chapter 4:

Design for reversible on-off regulation of volume oscillation by the magnetic field

4-1. Introduction

The reversible on-off regulation of the volume oscillation in self-oscillating hydrogels has been achieved by direct controls of the BZ reaction based on the kinetics[1-2]. However, the magnetic properties, i.e., magnetic responsiveness, can suggest an alternative to reversible on-off regulation of volume oscillation, which replaces a direct control of the BZ reaction, because it can lead to the anisotropic volume deformation of the hydrogel in the magnetic field without affecting the BZ reaction mechanism. The anisotropic deformation of the hydrogel by the magnetic field is achieved by cohesion of magnetic nanoparticles, which present in the hydrogel networks; therefore, the hydrogel networks are deformed such as the deswelling state of stimuli-responsive hydrogels. On the other hand, when the magnetic field is removed, the deformed hydrogel networks returns quickly to its original networks due to its elasticity[3]. Based on these, the reversible on-off regulation of the volume oscillation in self-oscillating hydrogel can be achieved depending on the on-off switching of the magnetic field (**Figure 4-1**).

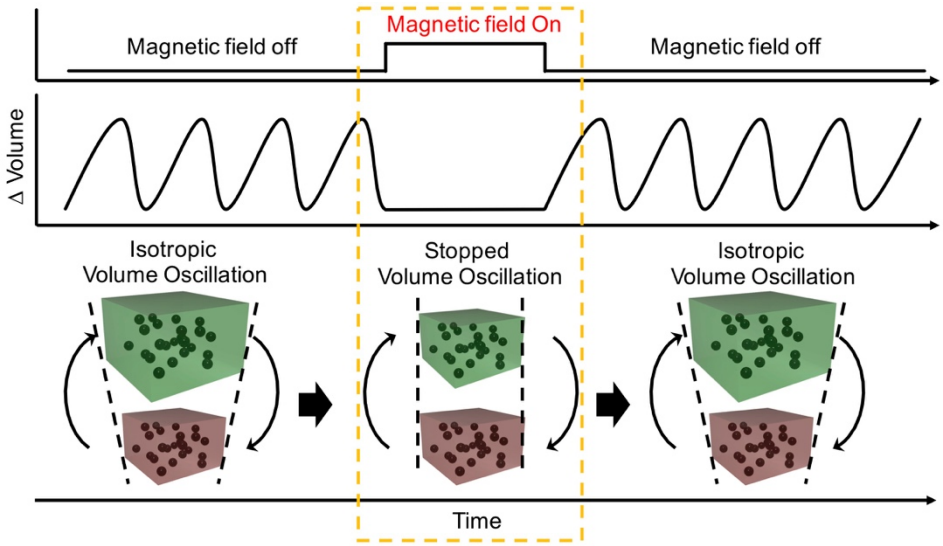

Figure 4-1. The schematic image of the reversible on-off regulation of volume oscillation in self-oscillating hydrogel by the magnetic field.

In order to achieve this concept, the magnetic deformation of the self-oscillating hydrogel should be performed with enough magnetic force more significant than the restoring force of elasticity, which is intended to return to the swelling state; i.e., it is required a large magnetic deformation. The deformation degree of magnetic hydrogels can be controlled by several factors related to the magnetic response[4]. In particular, the large deformation of the magnetic hydrogel can be induced by the representative two elements such as (1) the strong magnetic force controllable by the intensity of the magnetic field and the concentration of magnetic nanoparticles and (2) the large pore within hydrogels.

In order to the large magnetic-deformation of self-oscillating hydrogels, in this study, the hydrogel beads containing magnetic nanoparticles were introduced and were conjugated by cross-linkers to form the bulk-gel phase, as shown in **Figure 4-2**. When compared with the conventional self-oscillating hydrogel, the structure of the bulk-gel composed of hydrogel beads is more porous. Therefore, it can lead to the larger deformation than a conventional hydrogel due to the porous structure. Besides, the applying the reversible magnetic field is necessary for the reversible regulation. Therefore, the magnetic nanoparticles in the hydrogel beads are chemically bonded with hydrogel networks to prevent a damage from magnetic actions by the reversible magnetic field. By using the porous structure composed of hydrogel beads and the external magnetic field, the reversible on-off regulation of the volume oscillation was investigated.

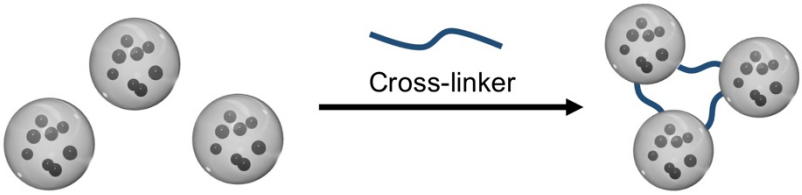

Figure 4-2. Preparation process of bulk-gel composed of hydrogel beads containing magnetic nanoparticles for making the porous structure.

4-2. Experiments section

4-2-1. Materials

N-isopropylacrylaminde (NIPAAm) was kindly provided by Kojin (Japan) and purified by recrystallization in toluene/n-hexane. *N*-(3-Aminopropyl) methacrylamide hydrochloride (NAPMAm) was purchased from Polyscience (USA) and used as received. *N,N'*-methylenebisacrylamide (MBAAm) was purchased form Acros Organics (Geel, Belgium) and used as received. Magnetic nanoparticles (soft ferrite) was kindly provided Powdertech (Japan) and used as received, and vinyl functionalized magnetic nanoparticles was prepared by protocol in the section 2-2-4. *N,N,N',N'*-tetramehtylethylendiamine (TEMED) and ammonium peroxide (APS) were purchased from Wako Pure Chemical Industries (Japan) and used as received. Bis (2,2'-bipyridine) (1-(4'-methyl-2,2'-bipyridine-4- carbonyloxy)-2,5-pyrrolidinedione) ruthenium(II) bis (hexafluorophosphate) (abbreviated as $Ru(bpy)_3$-NHS) was synthesized according to the previous report.[5] Sorbitan monostearate (Span 60) was purchased from Tokyo kasei and used as received. All other chemicals were purchased from Wako Pure Chemical Industries (Japan) and used as received.

4-2-2. Preparation of self-oscillating hydrogel beads containing magnetic nanoparticles by suspension polymerization

The hydrogel beads chemically containing magnetic nanoparticles were prepared by the inverse suspension polymerization using cyclohexane as the continuous phase (**Figure 4-3**), as previously reported[6]. The nonionic surfactant (Span 60) was dissolved in the cyclohexane at a 5 wt% concentration. And then, the 200 g of cyclohexane containing nonionic surfactant was transferred to the 500 mL water-jacket reactor set at 20 °C and was purged with dry Ar for 1 hour with mechanical stirring at 150 rpm. The

pre-gel solution was prepared by following protocol. the magnetic nanoparticles were suspended at a concentration of 60 mg/mL using the ultrasonication for 1 min, and then it was cooled down at 4 °C of the refrigerator for 1 hour. NIPAAm (509 mg, 9 mmol), NAPMAAm (89 mg, 1 mmol), APS (54 mg, 0.25 mmol), and MBAAm (8 mg, 0.1mmol) were dissolved in the 5 mL of prepared magnetic nanoparticles suspension, and the pre-gel solution was degassed by dry Ar gas. Before injecting a pre-gel solution into the reactor, the TEMED (332 μL) was injected into cyclohexane phase, and then the pre-gel solution was immediately injected into cyclohexane phase. The polymerization was allowed to proceed for 1 hour at 20 °C. After polymerization, the hydrogel beads were washed several times by the decantation in the ethanol, which can wash surfactants and cyclohexane. Finally, the separated hydrogel beads were dialyzed against the deionized water for 3 days and then freeze-dried.

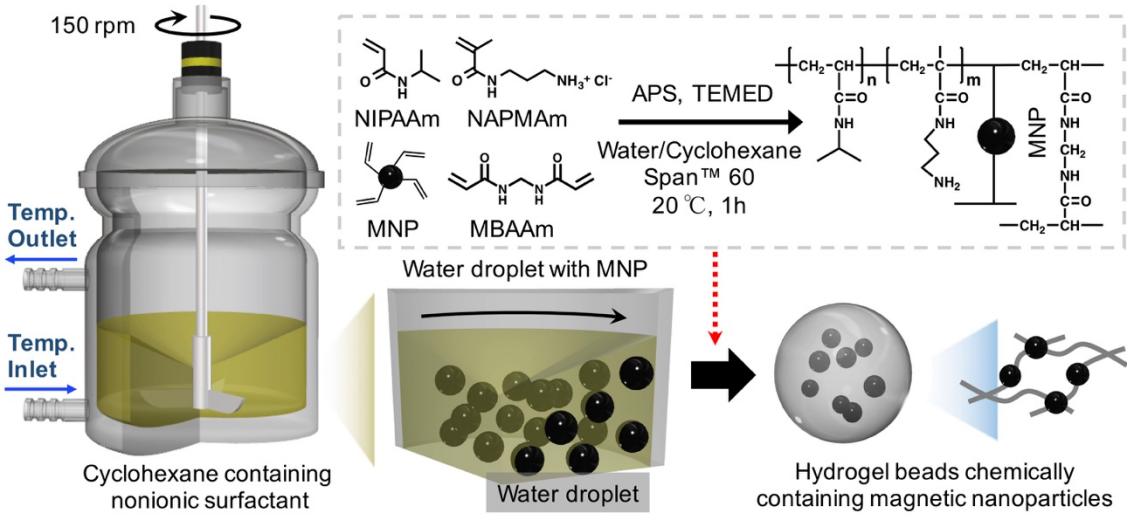

Figure 4-3. Schematic image for the preparation of hydrogel beads chemically containing magnetic nanoparticles by the inverse suspension polymerization.

Next, the $Ru(bpy)_3$-NHS was introduced into hydrogel beads. The 30 mg of freeze dried hydrogel beads were dispersed in 15 mL of DMSO for 2 days. 5 ml of DMSO with $Ru(bpy)_3$-NHS (50 mg, 0.05mmol) and triethylamine (TEA, 0.21 mL, 1.5 mmol) was mixed into the hydrogel beads and the mixture was stirred by rotator at room temperature for 2 days. The products were purified by dialysis against deionized water for 3 days.

4-2-3. Preparation of bulk-gel composed of self-oscillating hydrogel beads

The bulk-gel composed of self-oscillating hydrogel beads containing magnetic nanoparticles was achieved by the chemical conjugation between primary amine of hydrogel beads and NAS groups of cross linkers (P(DMAAm-*r*-NAS) prepared in Chapter 2 or Tetra-PEG_{20kDa}-NHS). First, the hydrogel beads containing magnetic nanoparticles were dispersed in PBS solution, and the cross-linkers was also dissolved in PBS solution. And then, the 0.5 mL of the cross-liker solution was transferred to a vial, and it was placed on the neodymium magnet (300 mT). Then the hydrogel beads dispersed solution was injected into a vial. The reaction was carried out for 3 hours; the products were washed with deionized water to remove unreacted cross-linker for 1 day.

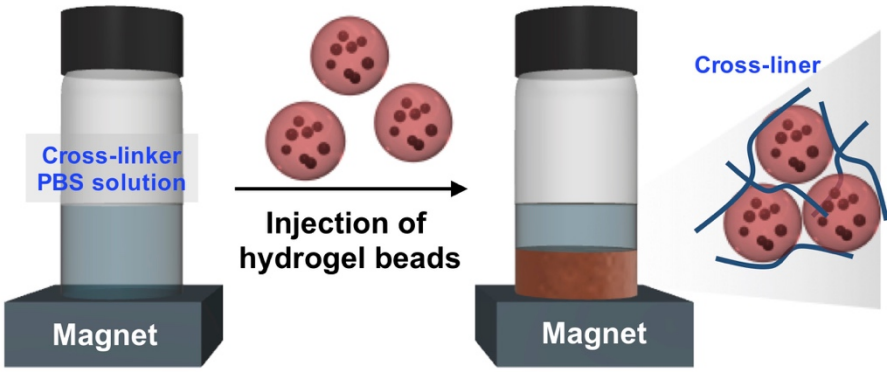

Figure 4-4. Schematic image for preparation of bulk-gel composed of self-oscillating hydrogel beads chemically containing magnetic nanoparticles.

4-2-4. Microscopic analysis of self-oscillating hydrogel beads containing magnetic nanoparticles

The prepared hydrogel beads were observed by optical microscopy (OLS4100, Olympus) to analyze the size of hydrogel beads and by fluorescence microscopy (DFC 360FX, Leica) (excitation wavelength, 425 nm; fluorescence wavelength, 585 nm) to confirm the introduction of $Ru(bpy)_3$, respectively. The optical images were converted into size distribution data by using the ImageJ (USA).

4-2-5. Observation of dynamic behaviors of bulk-gel composed of self-oscillating hydrogel beads containing magnetic nanoparticles

The bulk-gel composed of self-oscillating hydrogel beads containing magnetic nanoparticles was cut to a size of 2 x 2 x 1 mm^3 to observe the dynamic behaviors, and it was immersed in the solution containing 894 mM of HNO_3 and 84 mM of $NaBrO_3$ for 20 min, to make the network more hydrophilic through the oxidation of $Ru(bpy)_3$ moieties. And then, the oxidized hydrogel was placed in the petri dish with the BZ solution consisted of 894 mM of HNO_3, 84 mM $NaBrO_3$ and 62.5 mM of Malonic acid (MA), respectively. The external magnetic field was introduced by the neodymium magnet (530 mT) located below petri dish. The on-off regulation of magnetic field was carried out by manual control of magnet position. The dynamic behaviors with the on-off regulation of magnetic field were monitored at 10 seconds intervals by using an optical microscope system (Keyence VH-5500, Japan). The optical images were converted into time-course image of dynamic behaviors by using the ImageJ (USA).

4-3. Results and discussions

4-3-1. Preparation of self-oscillating hydrogel beads chemically containing magnetic nanoparticles by suspension polymerization

The polymer beads have been prepared by emulsion polymerization[7], suspension polymerization[8], precipitation polymerization[9], microfluidics[10], and water droplets on superhydrophobic surfaces[11], *etc.* In this study, the hydrogel beads were prepared by suspension polymerization because the magnetic nanoparticles located in the the mobile phase (water). The hydrogel beads chemically containing magnetic nanoparticles were designed to prevent a destruction of hydrogel networks by repetitive on-off regulation of magnetic field. In order to prepare the hydrogel beads chemically containing magnetic nanoparticles, the vinyl functionalized magnetic nanoparticles were suspended in the pre-gel solution. Although they can form the hydrogel networks with monomer without any cross-linker, it is difficult to assign the polymer networks for dynamic behavior by the BZ reaction. Therefore, the low-molecular weight cross-linker was introduced into the pre-gel solution. Finally, the hydrogel beads chemically containing magnetic nanoparticles could be obtained, as shown in **Figure 4-5a**. The average diameter of hydrogel beads was measured by 241 ± 138 μm. After post-conjugation of $Ru(bpy)_3$, the average diameter of self-oscillating hydrogel beads decreased to 172 ± 48 μm because $Ru(bpy)_3$ moieties of reduced state induced the hydrophobic hydrogel networks, as shown in **Figure 4-5b**. In addition, it was confirmed by the fluorescence image that the $Ru(bpy)_3$ moieties were homogeneously conjugated with the whole of hydrogel beads. The fluorescence image of self-oscillating hydrogel beads could provide the information to distinguish the binding types between magnetic nanoparticles and the hydrogel phase. In case of chemically bonded magnetic nanoparticles, the monomers are polymerized around vinyl functionalized magnetic

nanoparticles. Therefore, the polymer networks existed on the surface of hydrogel beads, and the fluorescence intensity was homogeneously observed after $Ru(bpy)_3$ moieties were conjugated with hydrogel networks. Conversely, in case of physically embedded magnetic nanoparticles, the magnetic nanoparticles could be placed anywhere on the surface of hydrogel beads as well as on the inside. Thus, the fluorescence intensity of $Ru(bpy)_3$ moieties was heterogeneously observed, as shown in **Figure 4-6**.

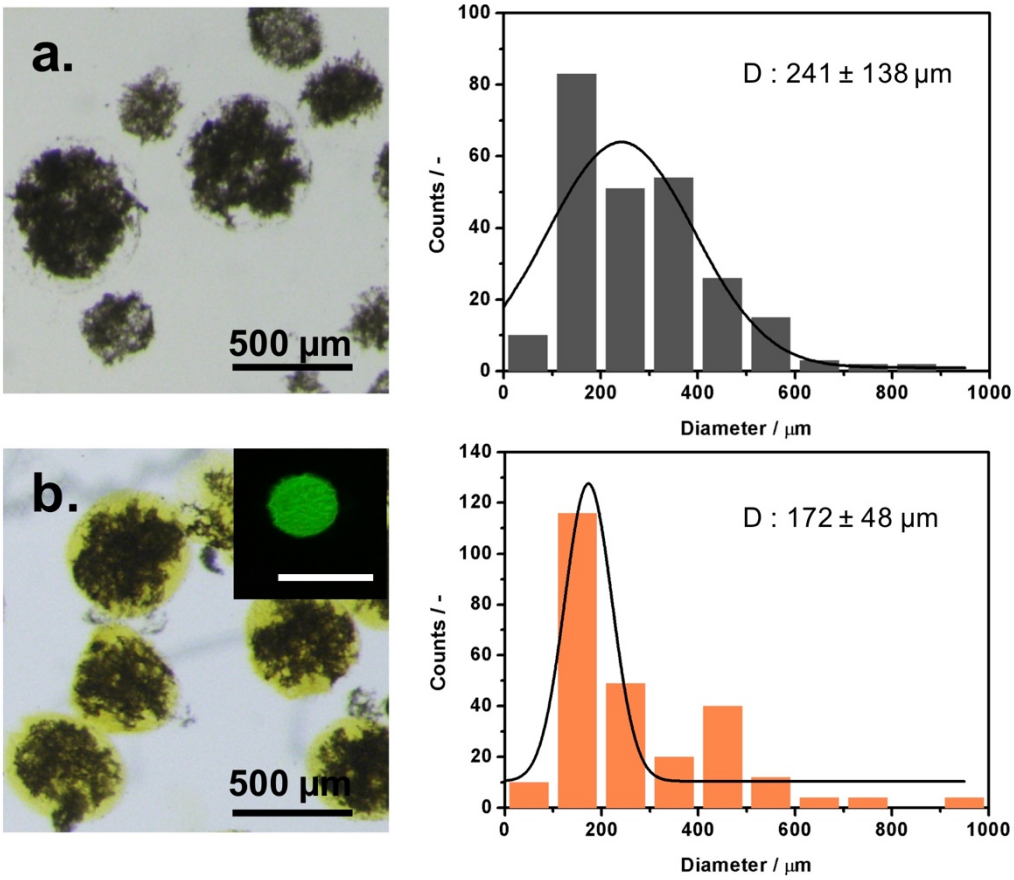

Figure 4-5. Microscopic images (left) and the distribution of the average diameter (right) of hydrogel beads chemically containing magnetic nanoparticles prepared within the 5 wt% Span 60 continuous phase. **(a)** hydrogel beads and (b) self-oscillating hydrogel beads, respectively. The inset image is the fluorescence image of self-oscillating hydrogel beads. (all scale bar: 500 μm)

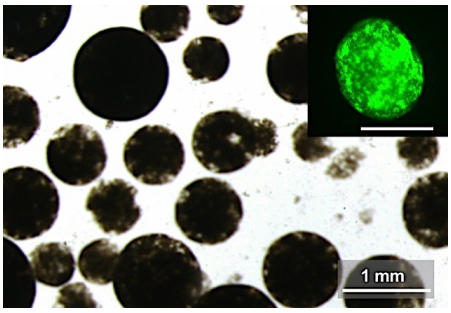

Figure 4-6. Optical and fluorescence (inset) images of hydrogel beads physically containing magnetic nanoparticles. The hydrogel beads were prepared within the 10 wt% Span 83 continuous phase and the average diameter was 676 μm. (inset scale: 500 μm)

4-3-2. Dynamic behaviors of self-oscillating hydrogel beads

The volume phase transition temperature (VPTT) was investigated in both of reduced and oxidized states for observing the dynamic behaviors of the prepared self-oscillating hydrogel beads, as shown in **Figure 4-7**. The redox state of oxidized $Ru(bpy)_3$ moieties within the hydrogel phase affects the hydrophilicity of the hydrogel; therefore, the average diameter of self-oscillating hydrogel beads shows a difference depending on their redox state. The swelling-deswelling oscillation of self-oscillating hydrogel beads can be observed at around 20 ºC due to the large gap between oxidized and reduced states.

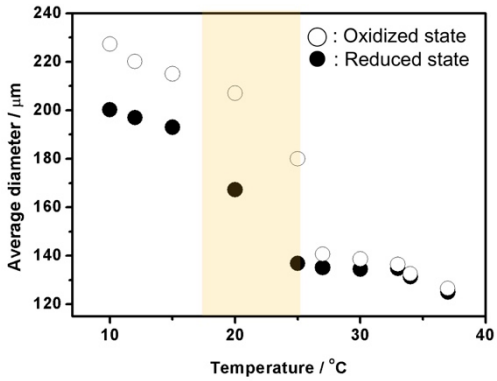

Figure 4-6. The equilibrium swelling ratio of self-oscillating hydrogel beads in the reduced and oxidized states as a function of temperature. (Oxidized state: $[HNO_3]$ = 894 mM, [NaBr03] = 84 mM, Reduced state: $[HNO_3]$ = 894 mM [NaCl] = 84 mM)

Therefore, the BZ reaction of single self-oscillating hydrogel beads was carried out under various reaction condition at 20 ºC, as shown in **Figure 4-7**. However, the self-oscillating hydrogel beads maintained a steady state, regardless of a sufficient reaction condition. The dynamic behaviors of self-oscillating hydrogels are generated by the diffusion of reaction intermediates within the hydrogel phase containing $Ru(bpy)_3$. However, micro-sized beads have a low concentration of $Ru(bpy)_3$, and the reaction intermediates are not sufficiently generated; Thus no significant oscillations were observed when a single hydrogel bead was reacted under various conditions for the BZ reaction. It is shown that it is important to form the bulk-gel composed of self-oscillating hydrogel beads for the dynamic behaviors.

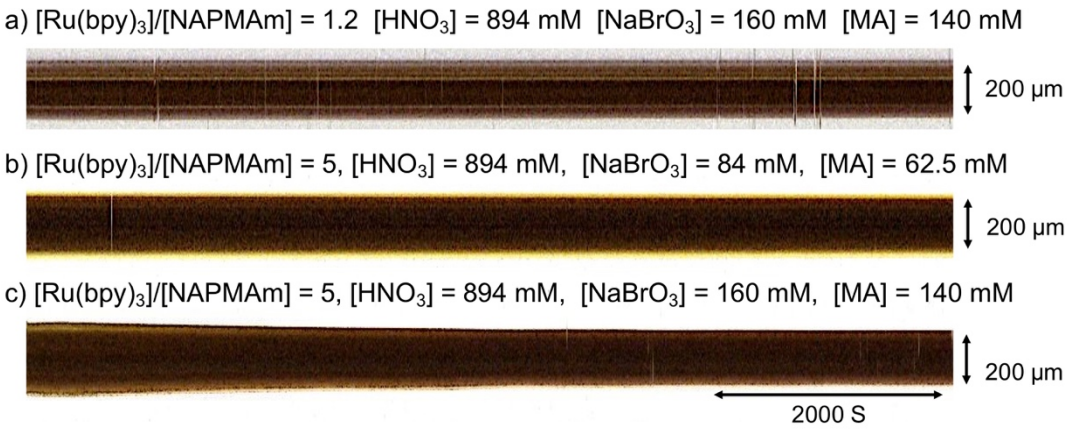

Figure 4-7. The dynamic behaviors of single self-oscillating hydrogel beads depending on the reaction conditions at 20 ºC.

4-3-3. Development of bulk-gel composed of hydrogel beads depending on the cross-linker types

The bulk-gel composed of hydrogel beads containing magnetic nanoparticles can be achieved by chemical conjugation between the amine groups onto hydrogel surface

and cross-linker having NAS groups, which can react with amine groups. Therefore, two factors, such as the amount of amine group and cross-linker types, was investigated for forming the bulk-gel composed of hydrogel beads. The amount of amine group was distinguished by the introduced $Ru(bpy)_3$, and two types of cross-linkers were characterized by linear and tetra types; it related to the distance between the chemical bonding site of cross-linker. The linear type has a 1.7 kDa, and Tetra type has the above 20 kDa. Therefore, the bulk-gels composed of hydrogel beads was carried out in these cases, as shown in **Table 4-1**. In these cases, the bulk-gel was only formed by simple hydrogel beads and the tetra types cross-linker, as shown in **Figure 4-8** The cross-linker must be connected between two hydrogel beads to form the bulk-gel phase. In the case of linear type cross-linker, the functional groups are relatively close together, and the hydrogel is bigger than the cross-linker when comparing the size of hydrogel beads and cross-linker. Therefore, it is difficult to connect between hydrogel beads because the cross-linkers are absorbed onto the surface of hydrogel beads.

In contrast, the tetra type cross-linker could form the bulk-gel phase because the functional groups are far enough apart. Besides, it is required enough amine groups onto the surface of hydrogel beads to form the bulk-gel phase. However, the tetra type cross-linker can be hydrolyzed in the BZ solution. Therefore, it is required that synthesis of the new tetra type cross-linking agents which do not undergo hydrolysis.

Table 4-1. The reaction condition to form the bulk-gel composed of hydrogel beads

	Beads type	Cross linker type
1	With $Ru(bpy)_3$	Linear type
2	With $Ru(bpy)_3$	Tetra type
3	Without $Ru(bpy)_3$	Linear type
4	Without $Ru(bpy)_3$	Tetra type

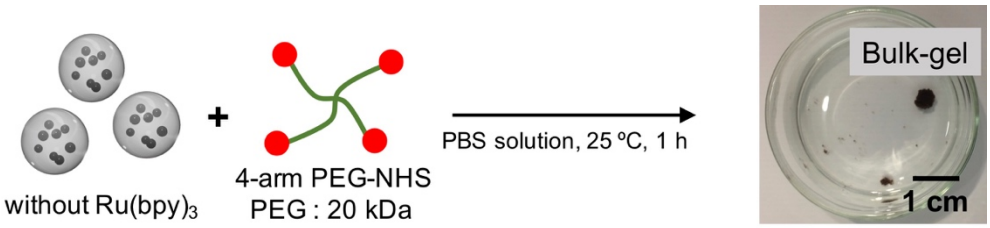

Figure 4-8. The preparing process of bulk-gel by using hydrogel beads and tetra type cross-linker and the image of the bulk-gel compose of hydrogel beads.

4-3-4. Magnetic responsiveness of hydrogel beads chemically containing magnetic nanoparticles

The prepared hydrogel beads chemically containing magnetic nanoparticles could be responded to the external magnetic field, as shown in **Figure 4-9**. The hydrogel beads could be cohered by the neodymium magnet (530 mT) as well as the magnetic deformation could be achieved when the on-off regulation of magnetic field was applied at 5 s intervals, even though they were not combined as the bulk-gel structure. The cluster composed of unlinked hydrogel beads can form a porous structure when the hydrogel beads were accumulated at the bottom; therefore, the porous structure could lead the magnetic deformation by the magnetic field. Besides, it showed the probability that the magnetic deformation of bulk-gel composed of self-oscillating hydrogel beads can be achieved by the applying the on-off regulation of magnetic field.

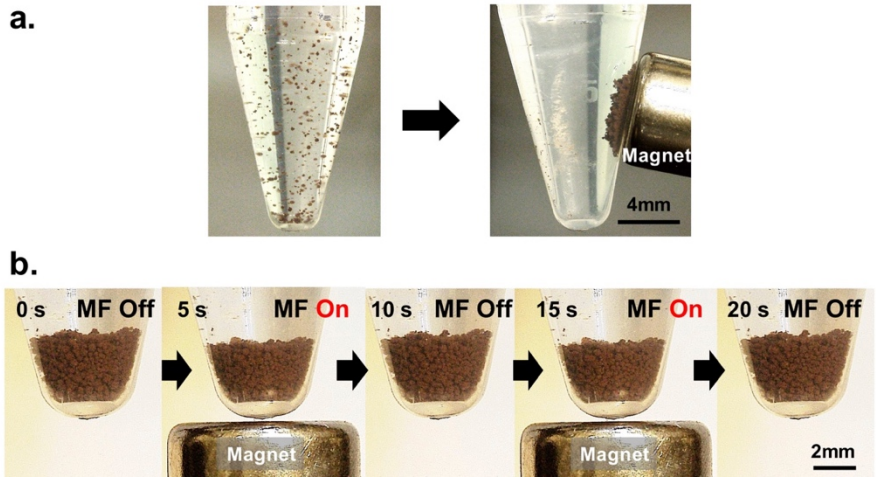

Figure 4-9. **(a)** The magnetic responsiveness of hydrogel beads containing chemically magnetic nanoparticles. **(b)** The magnetic deformation of the cluster composed of unlinked hydrogel beads chemically containing magnetic nanoparticles by the on-off regulation of the magnetic field (530 mT).

4-4. Conclusion

In this chapter, the reversible on-off regulation of volume oscillation in the self-oscillating hydrogels was attempted by the magnetic deformation, which can be observed in the porous magnetic hydrogels. Therefore, the hydrogel beads were introduced for inducing the magnetic deformation in self-oscillating hydrogel because the bulk-gel composed of hydrogel beads can be more porous structure than conventional hydrogels. Besides, for the magnetic deformation, it is necessary to introduce magnetic nanoparticles into hydrogel networks, and the chemical bond between magnetic nanoparticles and hydrogel networks is required to prevent damage caused by applying the reversible magnetic field. Therefore, the hydrogel beads chemically containing magnetic nanoparticles were prepared by inverse suspension polymerization. In this study, the cross-linker to form the bulk-gel phase was investigated. Although the bulk-gel could be prepared by tetra type cross-linker, it was required a new type tetra cross-linker to prevent

the hydrolysis in the BZ solution. Besides, the magnetic deformation in the cluster composed of unlinked self-oscillating hydrogel beads could be observed by the on-off regulation of the magnetic field.

Based on these results, it is expected that the bulk-gel composed of the linked self-oscillating hydrogel beads can achieve the magnetic deformation due to the porous structure; thus, it can suggest an alternative to reversible on-off regulation of volume oscillation in self-oscillating hydrogels, which replaces a direct control of the BZ reaction, by using the magnetic deformation.

4-5. References

[1] S. i. Shinohara, T. Seki, T. Sakai, R. Yoshida, Y. Takeoka, *Angew. Chem.* **2008**, *120*, 9179.

[2] R. Yoshida, K. Takei, T. Yamaguchi, *Macromolecules* **2003**, *36*, 1759.

[3] X. Zhao, J. Kim, C. A. Cezar, N. Huebsch, K. Lee, K. Bouhadir, D. J. Mooney, *PNAS* **2011**, *108*, 67.

[4] A. Khokhlov, Y. Osada, *Polymer gels and networks*, Marcel Dekker, **2002**.

[5] B. M. Peek, G. T. Ross, S. W. Edwards, G. J. Meyer, T. J. Meyer, B. W. Erickson, *Int. J. Pept. Protein Res.* **1991**, *38*, 114.

[6] M. Annaka, T. Matsuura, M. Kasai, T. Nakahira, Y. Hara, T. Okano, *Biomacromolecules* **2003**, *4*, 395.

[7] H. Hu, X. Wang, J. Wang, L. Wan, F. Liu, H. Zheng, R. Chen, C. Xu, *Chem. Phys. Lett.* **2010**, *484*, 247.

[8] P. J. Dowding, B. Vincent, *Colloids Surf. A* **2000**, *161*, 259.

[9] K. Yoshimatsu, K. Reimhult, A. Krozer, K. Mosbach, K. Sode, L. Ye, *Anal. Chim. Acta* **2007**, *584*, 112.

[10] C. A. Serra, Z. Chang, *Chem. Eng. Technol.* **2008**, *31*, 1099.

[11] A. C. Lima, W. Song, B. Blanco-Fernandez, C. Alvarez-Lorenzo, J. F. Mano, *Pharm. Res.* **2011**, *28*, 1294.

Chapter 5:

Concluding Remarks

5-1. Summary

The research approach of this dissertation is based on that the magnetic properties could provide an alternative to developing the self-oscillating hydrogel as smart materials without affecting the BZ reaction mechanism. Therefore, the final goal of this dissertation was to fabricate the self-oscillating hydrogel containing magnetic nanoparticles and to regulate dynamic behaviors, which appeared in the forms of the chemical wave propagation and the volume oscillation, by a magnetic field. To achieve the final goal of this dissertation, the author carried out researches and concluded them as followings.

In chapter 2., the preparation methods of self-oscillating hydrogels containing magnetic nanoparticles were investigated to overcome some drawbacks that represent in the conventional self-oscillating hydrogels. Therefore, it is achieved by the two types functional copolymers and surface modified magnetic nanoparticles. By using these, the self-oscillating hydrogels containing magnetic nanoparticles were prepared and were classified by the binding types between magnetic nanoparticles and the hydrogel networks. Each self-oscillating hydrogels containing magnetic nanoparticles will be applied from the next chapters depending on research objects.

In chapter 3., the directional control of chemical waves was investigated by magnetic migrations and liquid interfaces. The regularity in the propagation of chemicals waves could be observed in the reaction environments having liquid interface consisted of the aqueous BZ solution and organic solvents immiscible with water. By taking advantage of the regularity, it was introduced that the magnetic migration by self-oscillating hydrogels physically containing magnetic nanoparticles and three-layers system accumulated by utilizing density differences of each solvent. Therefore, the directional control was achieved by the magnetic migration in the three-layer system; the propagation directions were decided by the interface position immersed in BZ solution.

Beyond directional control of chemical wave propagation, it was possible to reversibly switch the direction of the chemical wave in a targeted way at a desired time by manipulating the position in the liquid system.

In chapter 4., the reversible on-off regulation of the volume oscillation in self-oscillating hydrogels was attempted by external magnetic field**.** In order to achieve this concept, it was designed that the bulk-gel was composed of self-oscillating hydrogel beads chemically containing magnetic nanoparticles to form the porous structure and to prevent damage caused by applying the reversible magnetic field. Therefore, the self-oscillating hydrogel beads were prepared by inverse suspension polymerization, and the cross-linker to form the bulk-gel composed of hydrogel beads was investigated. Finally, magnetic deformation was confirmed by unlinked hydrogel beads. Based on these, it is expected that the reversible on-off regulation of volume oscillation in self-oscillating hydrogels composed of hydrogel beads can be achieved by the magnetic field.

In conclusion, the magnetic properties can provide expended functionalities to self-oscillating hydrogels without affecting the BZ reaction mechanism. Therefore, the regulation of dynamic behaviors in self-oscillating hydrogels could be achieved by magnetic activation modes such as a magnetic migration and a magnetic deformation; these can lead the self-oscillating hydrogels evolved into smarter materials than now. Besides, it is expected that the self-oscillating hydrogel containing magnetic nanoparticles can be applied to other fields, which require magnetic properties, beyond the regulation of dynamic behaviors.

5-2. Future perspectives

In this chapter, the future perspectives of the self-oscillating hydrogels containing magnetic nanoparticles are described. The self-oscillating hydrogels containing magnetic

nanoparticles have a potential to develop into the energy conversion system, which converts from the chemical energy of BZ reaction to the electrical energy. The electrical energy is generally generated by the kinetic energy of turbine driven by various sources such as flowing water and wind, steam produced by combustion or nuclear fission. The kinetic energy of turbine drives the generator and converts the mechanical energy into electrical energy by electromagnetic induction based on Faraday's law, as shown in **Figure 5-1a**. Yun *et al*[1]. demonstrated the ferrodynamics energy harvesting system based on air-droplet movement. The air-droplet movement alters the position of aligned magnetic nanoparticles by the magnetic field, and they generate current by electromagnetic induction based on Faraday's law. However, it is required additional equipment (i.e., outside energy) such as air droplet generator, to generate current.

In contrast, the self-oscillating hydrogels can offer a change of magnetic field without outside energy sources due to their autonomous dynamic behaviors. Nakata *et al*. demonstrated the periodic reciprocating motion of self-oscillating hydrogel driven by the BZ reaction, as shown in **Figure 5-1b**. If the self-oscillating hydrogel can serve as a magnet, this periodic reciprocating motion can express the experiment of electromagnetic induction. The self-oscillating hydrogel acting as a magnet can be prepared by the introduction of magnetic nanoparticles such as hard ferrite with high remnant magnetization. Therefore, the preparation methods of the self-oscillating hydrogel containing magnetic nanoparticles, which provided in this study, can provide a good solution for introducing hard ferrite magnetic nanoparticles.

Based on these, the energy conversion system will be achieved by the self-oscillating hydrogel acting as a magnet and periodic reciprocating motion driven by the BZ reaction, as shown in **Figure 5-1c**. The magnetized self-oscillating hydrogel is periodically reciprocated around the solenoid; this dynamic behavior can generate

induced current based on Faraday's law. Besides, the intensity of induced current can be controlled by elements related to the Faraday's law such as the speed of the reciprocating motion, the magnetized intensity, and the solenoid structure (*e.g.*, diameter, winding number of coil).

Finally, the author believes that the self-oscillating hydrogel containing magnetic nanoparticles could be available as a more advanced system beyond this dissertation since magnetic properties can provide diverse properties.

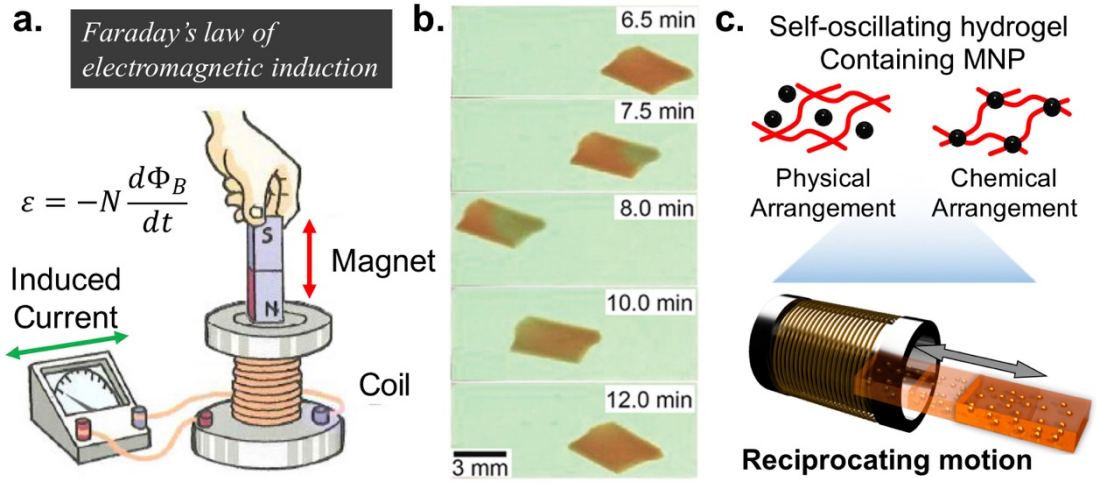

Figure 5-1. The concept of energy conversion system based on the dynamic behavior of self-oscillating hydrogel containing magnetic nanoparticles. **(a)** The schematic image of Faraday's law of electromagnetic induction, **(b)** the periodic reciprocating motion of the self-oscillating hydrogel[2], and **(c)** the schematic images of energy conversion system: the suggested hydrogel structures containing magnetic nanoparticles (upper) and the electromagnetic induction by the periodic reciprocating motion of the self-oscillating hydrogel containing magnetic nanoparticles (lower), respectively.

References

[1] H. R. Yun, D. J. Lee, J. R. Youn, Y. S. Song, *Nano Energy* **2015**, *11*, 171.

[2] S. Nakata, M. Yoshii, S. Suzuki, R. Yoshida, *Langmuir* **2014**, *30*, 517.

Appendix

A. List of publications

Original papers for the journal with peer review

1. **E. Lee**, Y. S. Kim, A.M. Akimoto, and R. Yoshida, Reversible and directional control of chemical wave propagation in a hydrogel by magnetic migration through liquid interfaces, *Chem. Mater*. Revised manuscript submitted

B. List of presentations

International conference

1. **E. Lee**, Y. Kim, A. M. Akimoto, R. Yoshida, *The 11th International Gel Symposium, 2017*, Nihon University, Chiba, Japan, (Mar. 2017) (poster)

Domestic conference

1. **E. Lee**, Y. Kim, A. M. Akimoto, R. Yoshida, 66th The society of polymer science, Japan (SPSJ) annual meeting, Makuhari Messe, Chiba, Japan, (May. 2017) (poster)

2. **E. Lee**, Y. Kim, A. M. Akimoto, R. Yoshida, 66th Symposium on Macromolecules, Ehime University, Ehime, Japan, (Sep. 2017) (poster)

C. Awards

1. 66th The society of polymer science, Japan (SPSJ) Annual Meeting: **Best poster award** (May. 2017)